

June 2021

Oxygen diffusion in saturated covers



**Yukon
University**

Project Team

Roselyne Gagné Turcotte

Dr. Guillaume Nielsen

Dr. Nicolas Reynier

Ayesha Waqar Ahmad

Université Laval

YukonU Research Centre

NRCAN

YukonU Research Centre

Acknowledgments

We would like to thank NRCAN and CANMET Mining for their expertise and their contribution to this document until section 5. We also would like to thank CASINO Mining for their support. As well as Mary Mioska and Paul West-Sells for their help in editing and formatting this document.

[This publication may be obtained online at yukonu.ca/research](http://yukonu.ca/research)

This publication may be obtained from:

YukonU Research Centre, Yukon University

520 University Drive

P.O. Box 2799,

Whitehorse, Yukon

Y1A 5K4

(867) 668-8895

1-800-661-0504

yukonu.ca/research

Table of Contents

1	Introduction	1
2	Theoretical Considerations.....	2
2.1	Unfrozen Porous Media.....	2
2.2	Effective Diffusion and Reaction Rate	3
2.3	Experimental Methods to Determine Oxygen Flux.....	3
2.3.1	Diffusion-Consumption Cell Method.....	4
2.3.2	Gradient Method	5
2.3.3	Sulphate Method	5
2.3.4	Method Comparison.....	6
3	Literature Review	6
3.1	Frozen Partially Saturated Porous Media	9
3.1.1	Estimation of the diffusion coefficient in partially saturated and frozen porous media.....	9
3.1.2	Estimation of the reaction rate coefficient in partially saturated and frozen porous media ..	10
4	Experimental Design	11
4.1	Objectives	11
4.2	Material and Methods.....	12
4.2.1	Cover material	12
4.2.2	Column set-up	12
4.2.3	Parameter monitoring.....	13
4.3	Experimental Protocol	14
5	Interpretation of the Results	15
5.1	Data Analysis and Unfrozen Volumetric Water Content	15
5.1.1	Case Scenario 1 - Low Water Level.....	15
5.1.2	Case Scenario 2 - Mid Water Level	18
5.1.3	Case scenario 3: High Water Level (Above port 4)	21
5.1.4	UVWC Analysis:	24
5.2	O ₂ Concentration and Temperature	25
5.2.1	First Cycle: Low water level (Between port 1 and port 2).....	25
5.2.2	Low water level: Unfrozen volumetric water content and O ₂ concentration	26
5.2.3	Second Cycle: Mid water level (between port 2 and 3) Upper O ₂ sensor	26

5.2.4	Second Cycle: Mid water level (between port 2 and 3) Lower O ₂ sensor.....	27
5.3	O ₂ Data Analysis	28
6	Conclusions	28
6.1	Limitations.....	28
6.2	Summary of Results	28
6.3	Conclusions	29
6.4	Subsequent Experiment.....	29
7	References	30

List of Figures

Figure 1:	Single chamber consumption cell (Cossett, 2009)	4
Figure 2:	double-chamber diffusion-consumption cell (Cossett, 2009).....	5
Figure 3:	Experimental Column Set-up (from MEND, 2001)	7
Figure 4:	Dissolved Oxygen (mg/L) profiles, day 100 (from MEND, 2001)	8
Figure 5:	Effect of temperature on the flux of oxygen (Coulombe, 2012)	11
Figure 6:	Experimental setup	13
Figure 7:	Instrumented columns	14
Figure 8:	Case scenario involving different water table height	15
Figure 9:	Case Scenario 1 - water content measured at Port 1 (submerged) during (a) freeze & (b) thaw	16
Figure 10:	Case Scenario 1 - water content measured at Port 2 (un-submerged) during (a) freeze & (b) thaw	16
Figure 11:	Case Scenario 1 – water content measured at Port 2 (unsubmerged) during (ai) freeze & (bi) thaw, with a focus on the unfrozen water level increase and decrease	17
Figure 12:	Case Scenario 1 - water content measured at Port 3 (un-submerged) during (a) freeze & (b) thaw	17
Figure13:	Case Scenario 1 - water content measured at Port 4 (un-submerged) during (a) freeze & (b) thaw	18
Figure 14:	Case Scenario 2 - water content measured at Port 1 (submerged) during (a) freeze & (b) thaw	19
Figure 15:	Case Scenario 2 - water content measured at Port 2 (submerged) during (a) freeze & (b) thaw	19
Figure16:	Case Scenario 2 - water content measured at Port 3 (un-submerged) during (a) freeze & (b) thaw	20

Figure 17: Case Scenario 2 - water content measured at Port 4 (un-submerged) during (a) freeze & (b) thaw 20

Figure18: Case Scenario 3 - water content measured at Port 1 (submerged) during (a) freeze & (b) thaw 21

Figure19: Case Scenario 3 - water content measured at Port 2 (submerged) during (a) freeze & (b) thaw 22

Figure20: Case Scenario 3 - water content measured at Port 3 (submerged) during (a) freeze & (b) thaw 22

Figure21: Case Scenario 3 - water content measured at Port 4 (submerged) during (a) freeze & (b) thaw 23

Figure 22: Data comparison of all 4 ports and all three water levels 24

Figure 23: First cycle, low water level, Upper O2 in freezing conditions: (a) Upper O2 sensor, (b) Lower O2 sensor 26

Figure 24: Second cycle, mid water level, Upper O2: (a) freeze, (b) thaw..... 27

Figure 25: Second cycle, mid water level, Lower O2: (a) freeze, (b) thaw 27

List of Appendices

Appendix A: Unfrozen Saturated Media Equations..... 34

Appendix B: Unfrozen Unsaturated Media Equations..... 35

Appendix C: Double-Chamber Cell Design 0

List of Acronyms and Abbreviations

ABS	Acrylonitrile-Butadiene-Styrene
AEV	Air entry value
AMD	Acid Mine Drainage
CEBC	Capillary effect barrier covers
D_e	Effective diffusion coefficient
DO	Dissolved oxygen
FVAC	Frozen volumetric air content
K_r	Reaction rate coefficient
MEND	Mine Environment Neutral Drainage
PVC	Polyvinyl Chloride
UVWC	Unfrozen volumetric water content
WEV	Water entry value

1 Introduction

Mine wastes are an important by-product of the mining industry, resulting from mineral resource extraction and mineral processing. Given their potential reactivity, however, they may pose significant risks to the environment if not properly managed. Considering that North America hosts the majority of new and closed mine sites, it is rather important to conduct research that focusses on mine waste management in Northern climates (MEND, 2006). Acid mine drainage (AMD) is a product of inadequate management of mine wastes (e.g., waste rock, tailings) containing sulphidic minerals (pyrite, pyrrhotite, chalcopyrite, etc.), common to copper, gold, nickel, coal, lead, uranium, iron and zinc extraction (Pétel, 2017). AMD occurs when sulphur present in sulphidic mine tailings is exposed to both oxygen and water. The subsequent leachate is characterized by a very low pH, a high electrical conductivity and a high concentration of sulphates and heavy metals.

Typically, mine waste management is focused on the elimination of at least one of the parameters responsible for sulphide oxidation: sulphides, water or oxygen. In Canada, oxygen barriers are often preferred (Ouangrawa, 2007), which include aqueous covers, saturated covers, and capillary effect barrier covers (CEBCs). An aqueous cover is ponded water of a given depth covering the mine wastes, while a saturated cover involves raising the water table into a dry cover installed on the mine waste surface; this cover can be either monolayer or multilayer and helps limit interactions with the atmosphere, such as evapotranspiration. CEBCs limit the supply of oxygen and water to the tailings by covering the coarse tailings with a fine-grained soil that promotes water-retention (Aubertin et al., 2009).

Saturated covers are designed to minimize the diffusive flux of oxygen, thereby limiting the quantity of oxygen that reaches the potentially reactive mine wastes. Several well-documented techniques can be used in order to determine these fluxes, including the oxygen gradient method, the consumption-diffusion cell test method, and the sulphate method. However, these methods have been developed for the determination of oxygen fluxes at temperatures above freezing. Consequently, the migration of oxygen during periods of sub-zero temperatures is an occurrence often neglected in studies. Although studies have shown that the diffusion and consumption of oxygen are both significantly reduced at lower temperatures, their impact on the flux of oxygen through the cover has not been well studied.

The monolayer saturated cover would allow for the storage of de-pyritized tailings, as well as the consumption of some of the oxygen diffusion through the saturated cover; this will be beneficial as long as the cover itself does not generate acidity and excludes metals from the leachate. It should also be noted that mine tailings often have favorable hydrogeological characteristics for their use as a cover material, particularly in regards to their low permeability. Several studies confirm their effectiveness in preventing AMD (Demers et al., 2010; Bussière et al., 2004; Gosselin, 2007; Mbonimpa et al., 2011).

The objective of this study is therefore to evaluate the impact of freeze-thaw cycles on oxygen migration within saturated covers over tailings, by simulating a tailings cover system in the laboratory through column experiments. Covers for waste rock are not evaluated, but may be the topic of future research. This report details the selection of experimental methodology, background literature, experimental design, and details the results of the column experiments.

2 Theoretical Considerations

In order to study the mechanisms that govern the transport of oxygen through saturated cover material and reactive tailings, a good understanding of the physical and chemical laws explaining the behavior of water and gases in saturated and partially saturated media is necessary. Partially saturated (or unsaturated) and unfrozen porous media flow is more complex due to the presence of all three phases (solid, liquid and gas). This “vadose zone” area (located above the water level), when combined with a solid phase characterized by the presence of sulphides (iron sulphide, for example), is where the geochemical processes driving AMD occur.

Theoretical information sourced from previous research on oxygen transport, which has been used to inform the selection of methodology for the research project described herein, is summarized in the following subsections. The equations that describe the behavior of water in an unfrozen saturated media are presented in Appendix A. The equations associated with the transport of water in unsaturated and unfrozen porous media, along with associated parameters, are presented in Appendix B.

2.1 Unfrozen Porous Media

In order to investigate the mechanisms driving oxygen diffusion in unfrozen unsaturated porous media during freezing temperatures, first, an understanding of the transport of oxygen, and molecular diffusion, through *unfrozen* unsaturated and saturated porous media is required, as the two states are homologous up to a certain point.

Caused by a concentration or partial pressure gradient, molecular diffusion is a phenomenon that tends to homogenize the spatial distribution of molecules until an equilibrium is reached (Hillel, 1998). Studies of oxygen migration through saturated cover material (characterized by fine particle size and a relatively low degree of saturation) point to the fact that molecular diffusion is the main mechanism of oxygen transport for the production of AMD (Collin, 1987, Nicholson et al., 1989, Mbonimpa et al., 2003, Demers, 2010). However, other mechanisms such as advection may not be negligible under transient or other specific conditions (Binning et al., 2007).

The determination of the unidimensional oxygen diffusive flux, generally expressed in $\text{mol} \cdot \text{m}^{-2} \cdot \text{year}^{-1}$, can be calculated from Fick’s first law of diffusion (Mbonimpa et al., 2003, Aachib et al., 2004, Mbonimpa et al., 2011), as:

$$F(z, t) = -D_e \frac{\partial C(z, t)}{\partial z} \quad (\text{Equation 1})$$

Where F is the diffusive flux of oxygen [$\text{ML}^{-2}\text{T}^{-1}$ or $\text{mol L}^{-2}\text{T}^{-1}$], D_e is the effective diffusion coefficient [L^2T^{-1}], C is the concentration of molecular oxygen [ML^{-3} or mol L^{-3}], z is the depth [L] and t is the time [T].

In the case of materials that react with oxygen such as pyrite, it is also necessary to consider the consumption of oxygen associated with the oxidation reactions, in addition to diffusion. Assuming that the oxidation reactions of sulphide minerals can be considered as first-order kinetic reactions (linear proportionality ratio between the speed of consumption of O_2 and its concentration [Nicholson et al., 1988]), these can be integrated in Fick’s second law of diffusion via the coefficient of the reaction rate K_r (Mbonimpa et al., 2002, 2003):

$$\theta_{eq} \frac{\partial C}{\partial t} = D_e \frac{\partial^2 C}{\partial z^2} - K_r C \quad (\text{Equation 2})$$

Where θ_{eq} is the equivalent porosity [L^3L^{-3}], K_r is the reaction rate coefficient [$L^3L^{-3}T^{-1}$ or $MM^{-1}T^{-1}$].

Equivalent porosity can also be expressed as:

$$\theta_{eq} = \theta_a + H\theta_w \quad (\text{Equation 3})$$

Where H is Henry's constant at a given temperature, θ_w is the volumetric water content and θ_a is the air volume content. θ_w and θ_a are both derived from the water retention curve, detailed in Appendix B. In the presence of an inert material, the second term of the equation associated with the coefficient of the reaction rate ($K_r C$) is then equal to 0.

2.2 Effective Diffusion and Reaction Rate

The effective diffusion coefficient and coefficient of reaction rate are two of the most important parameters of influence in the mathematical determination of oxygen flux in a fine grained and porous medium, such as mine tailings.

The effective diffusion coefficient (D_e) tends to decrease with an increase in water saturation, due to the lower diffusivity and solubility of gaseous oxygen in water (Yanful, 1993, Aachib et al., 2004). Several authors, have worked to adapt empirical or semi-empirical models to estimate D_e (Marshall, 1959, Millington and Quirk, 1961, Millington and Shearer, 1971, Collin, 1987, Aubertin et al., 1999, Mbonimpa et al., 2003, Aachib et al., 2004 and Nyameogo, 2017), however, limitations have been generally identified with these predictive models. These limitations, briefly discussed in Section 3.1, are important to assess, since a poor estimation of D_e will likely cause a significant error in the calculated oxygen flux. To determine an accurate D_e value, it is generally appropriate to conduct laboratory tests such as the diffusion consumption cell method, detailed in Section 2.3.1. Tortuosity, which is the ratio between the actual distance traveled and the shortest distance between two points, greatly influences D_e and is difficult to predict, hence should also be determined using laboratory methods.

The reaction rate coefficient, K_r , is also dependent on several physical characteristics, such as the mineralogy of the mine waste (type, quantity of metal sulphides and ferric ion concentration), the grain size distribution and the porosity of the medium, as well as the volumetric water content (θ_w). The volumetric water content influences the rate of diffusion of oxygen and therefore the reactivity of sulphurous minerals. The study by Gosselin (2007) shows that the reaction rate coefficient can be strongly influenced by the degree of saturation and tends to diminish with an augmentation of the degree of saturation. Other factors such as bacterial activity and temperature can also affect the reaction rate coefficient. Indeed, according to Nyameogo (2017), the reaction rate would become 23 times lower in the presence of frozen tailings (-11°C) than when it is determined at room temperature (21°C).

2.3 Experimental Methods to Determine Oxygen Flux

Three major experimental methods are typically used to determine oxygen fluxes: the diffusion-consumption cell method, the oxygen gradient method, and the sulphate method. These three methods are described below, with the most relevant and appropriate chosen for the proposed laboratory column experiments.

2.3.1 Diffusion-Consumption Cell Method

The diffusion consumption cell test is the most common experimental method to determine coefficients D_e and K_r , and comprise 3 main experiments: single-chamber cell test (to determine K_r), double-chamber cell test (for D_e and K_r determination), and column tests (for D_e and K_r determination).

The single chamber cell test is illustrated in Figure 1. In this test, a sample of material is deposited at the bottom of a sealed cell equipped with an oxygen sensor. Prior to the test, nitrogen is used to purge the oxygen out of the cell. At the beginning of the test, air is injected into the source reservoir and then saddled to measure the decrease in oxygen concentration measured over time. Software (e.g., POLLUTE or Vadose/W) can then be used to derive the coefficient K_r from the oxygen concentration versus time curve (Barbour et al., 1996; MacKay et al., 1998; Shelp & Yanful, 2000).

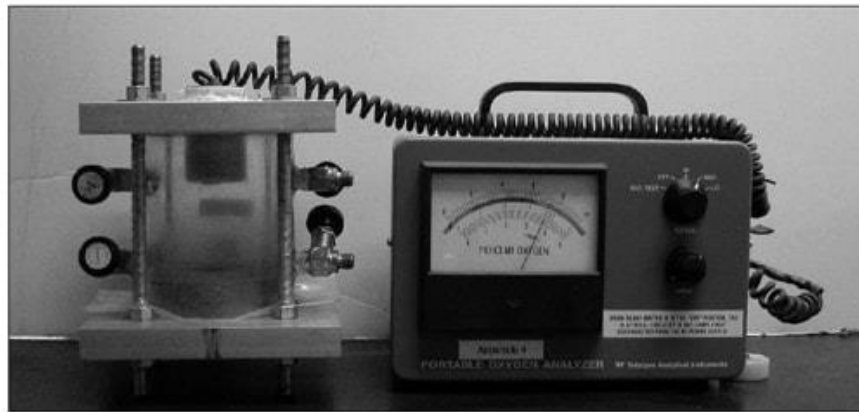


Figure 1: Single chamber consumption cell (Cossett, 2009)

The double-chamber diffusion-consumption test is slightly more complex. The sample is dried in a nitrogen chamber and brought to the desired density and water content, and is then placed on a perforated plate and two reservoirs are placed on either side of the material sample (Figure 2). The oxygen is removed from the cell and then re-introduced into the upper reservoir. Similar to the single-chamber test, the oxygen sensors placed in the two reservoirs make it possible to create the oxygen concentration curves as a function of time. D_e and K_r (if the material is not inert) can then be determined numerically (Yanful, 1993, Aubertin et al., 2000, Aachib et al., 2004) or analytically (Sallam et al., 1984, Glauz & Rolston, 1989, El-Farhan et al., 1996). According to Cossett (2009), the prediction of K_r values by double-chamber cell tests, however, tend to overestimate the value of this coefficient in some cases. This test would presumably not effect the obtained value of D_e but may results in uncertain K_r determination, particularly given the fact that it is difficult to control the density and the degree of saturation of the sample very precisely (Gosselin, 2007). For this reason, single-chamber consumption tests are more accurate in determining K_r .

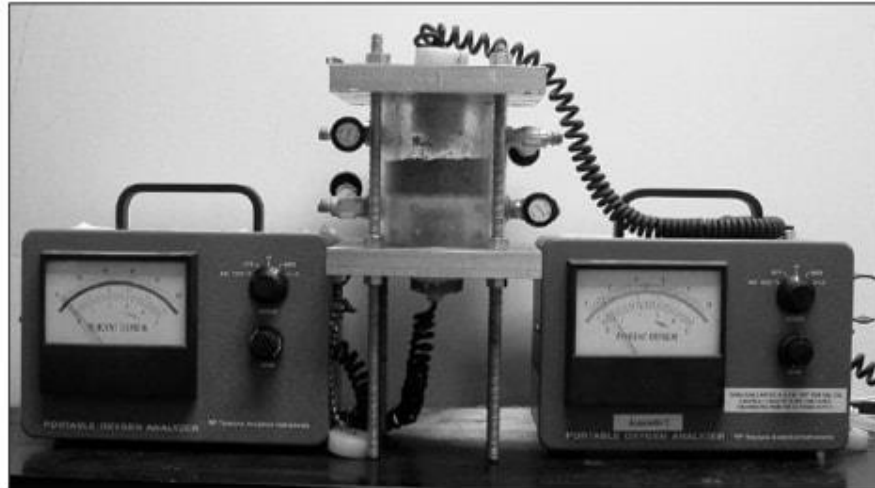


Figure 2: double-chamber diffusion-consumption cell (Cossett, 2009)

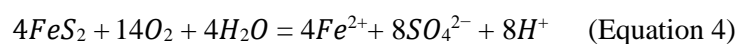
Elberling et al. (1994) proposed a similar method to the single-chamber test, but used instead a larger column and thicker sample of material cover (i.e., greater than the 2 cm initially proposed). This method exposes a material filled column to air until equilibrium is reached, then the upper reservoir is sealed (Gosselin, 2007, Mbonimpa et al., 2011). From the oxygen concentrations measured in the upper reservoir, it is once again possible to determine the coefficient K_r by using numerical methods.

2.3.2 Gradient Method

The gradient method is the most direct method. The gradient method applies Fick's first law of diffusion according to the measured O_2 concentrations at different depths. The oxygen concentration profile is obtained from the instrumented columns, which results in an oxygen concentration gradient in the cover and/or the reactive waste. This method requires the D_e and K_r values determined either from the diffusion-consumption cell test or from a predictive model. The calibration of a numerical model (the superposition of the values predicted by the software with those measured) makes it possible to model different fluxes for different timelines. An adapted method of this test can also be used in the field at full scale installations, for either inert or reactive covers, and at steady state conditions.

2.3.3 Sulphate Method

The sulphate method consists of deducing the amount of oxygen that has been consumed by the oxidation reaction of sulphide minerals (the amount of oxidized sulphur) from the amount of sulphate formed in the leachate (Elberling et al., 1994; David & Nicholson, 1995, Bussière et al., 2004). As shown in Equation 4, if we take the example of pyrite, for a relatively neutral pH (greater than 5), for every mole of sulphate formed, 1.75 moles of oxygen would be consumed:



The stoichiometric ratio obtained then makes it possible to convert the flux of sulphates measured into an oxygen flux. However, this method considers only direct oxidation because when the pH is too low, ferric

ions (produced from bacterial activity, for example) could compete with oxygen as an oxidizing agent. However, this method remains sensitive to certain influences, such as the precipitation of secondary sulphate minerals, which could result in a reduction in the amount of sulphate measured in the effluent and therefore an underestimation of the amount of oxygen consumed. Conversely, mineral dissolution of minerals containing primary sulphates such as gypsum, would have the opposite effect, resulting in an overestimation of the amount of oxygen consumption (Demers, 2008). This method may produce results that underestimate oxygen fluxes when using highly sulphurous materials, but is more accurate in the case of low sulphide tailings (Bussière et al., 1998).

2.3.4 Method Comparison

Several authors have sought to compare these three methods in order to identify their respective strengths and weaknesses. Elberling et al. (1994) compared the fluxes of oxygen obtained via the three methods in the field and in the laboratory. Although the results are relatively consistent, each method has its own limitations: in the diffusion-consumption cell test, very small changes in oxygen concentration may result in values below the limit of detection, which could falsely result in zero oxygen flux; thus, in the case of small oxygen fluxes, the use of the sulphate method is usually preferred (Bussière et al., 2004). However, geochemical conditions tend to influence the results obtained via the sulphate method. The precision of the results obtained by the gradient method is highly dependent on the accuracy of the estimate of the D_e coefficient.

For the current study, it was initially decided to use the gradient method to assess oxygen flux. Indeed, this method was assumed to be the most direct method that applied Fick's first law of diffusion according to the measured O_2 concentrations at different depths. As D_e and K_r are required in the gradient method, they were supposed to be determined by experimental measurements described in the proposed experimental protocol section (section 4).

3 Literature Review

Several characteristics of saturated covers have been identified in the literature as having an impact on oxygen flux, largely related to the efficiency of the saturated cover under review. Among these are the amount of sulphides, the degree of saturation, the grain size distribution and the type and thickness of the saturated cover. Although most studies are based on results obtained by numerical modeling of environmental conditions, a minority of them are derived from laboratory or field studies; pertinent studies are discussed below.

In a study by Demers et al. (2010), the effectiveness of a monolayer cover composed of tailings with a low residual sulphide content was investigated in the laboratory, at room temperature, according to three parameters: the level of the water table, which strongly influences the degree of saturation; the residual sulphide content in the cover material, 0.25 wt.% versus 1.24 wt.%; and thickness of the cover. For this study, the gradient method was chosen initially, and the coefficients D_e and K_r were supposed to be calculated.

Several conclusions can be drawn from this study: although the oxygen concentrations are relatively consistent throughout the test, even after several wetting and drying cycles, the measured oxygen concentrations increased over time, probably due to the decreased reactivity of the sulphide surfaces.

Overall, the lowest flux was measured for a sulphide doped cover (1.24% sulphide), with calculated values as low as $0.01 \text{ mol m}^{-2} \text{ year}^{-1}$. At the saturation level, as observed by Gosselin (2007), the K_r coefficient decreases with an increase in saturation to obtain very low values when saturation levels above 80% are used. In the case of a very low water level (1.3 meters under the reactive tailings-cover interface), the oxygen flux is approximately 10 times higher than in the reference case, where the water level was located at the tailings-cover interface. This result was related to the fact that for a low water table, the cover material is slightly drier and thus allows more oxygen to pass through the cover to reach the tailings, although some of the diffused oxygen is consumed by the sulphide minerals present in the cover material. In short, as the degree of saturation is increased, D_e would decrease rapidly and thus significantly reduce the calculated diffusive oxygen fluxes. The thickness of the cover results in higher oxygen fluxes and a steeper concentration distribution profile.

Another laboratory study by Bussière et al. (2004) also confirmed the effectiveness of covers composed of low-sulphide tailings (Bussière et al., 2004). Using the sulphate method, the author obtained oxygen fluxes at the surface of 10, 25 and $35 \text{ mol m}^{-2} \text{ year}^{-1}$ for sulphide contents of 0.22%, 0.65% and 1.17%, respectively. The estimated analytical fluxes at the base of the cover were 0.64, 0.06 and $0.08 \text{ mol m}^{-2} \text{ year}^{-1}$. The observed differences were due to oxygen consumption by the sulphides present in the cover material.

Similarly to Demers (2008), Ouangrawa (2007) tried to evaluate the impact of water table levels on oxidation of two mine tailings with inert covers. The results were obtained from large instrumented columns, by the sulphate method, and numerically using POLLUTE software. According to the author, the oxygen flux could be reduced from $2500 \text{ mol m}^{-2} \text{ year}^{-1}$ to $10 \text{ mol m}^{-2} \text{ year}^{-1}$ when the water level was raised to a value of at least 0.5 times the Air Entry Value (AEV) of the cover material (see Appendix B for more details on the AEV). In such a scenario, the oxidation rate would be very low. These experiments were also used to calibrate a numerical model using the MIN3P software which, based on long-term, 100-year predictions, would indicate that the elevated water table method combined with an inert monolayer cover would be effective in limiting the AMD phenomenon.

The Mine Environment Neutral Drainage (MEND) 2.12.1e report (MEND, 2001) presents the dissolved oxygen (DO) profiles measured for different submerged cover scenarios (Figure 3) under a circulated water cover at room temperature (Figure 4).

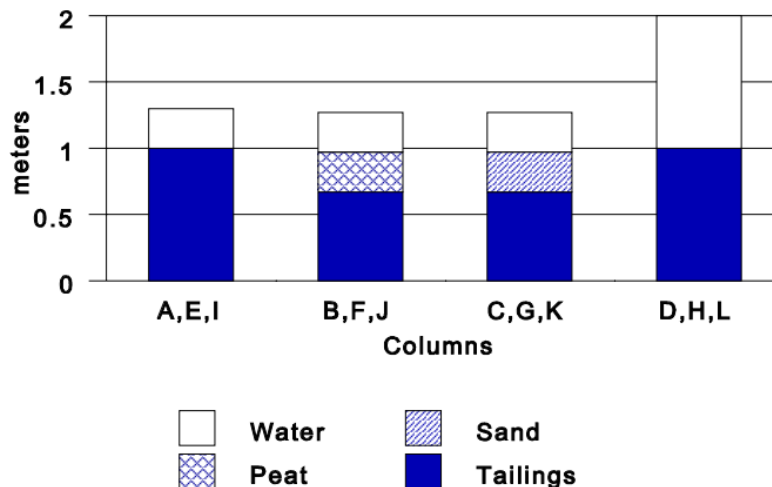


Figure 3: Experimental Column Set-up (from MEND, 2001)

From the concentration profiles measured on the 100th day (Figure 4), no significant DO gradient could be established in the overlying water of the column, confirming the results obtained previously by Davé et al. (1996) which describe the depth of the overlying water as irrelevant in their contribution to limiting the quantity of DO. Also, contrary to expected results, the sand consumed oxygen faster than peat. This was probably due to the fact that the peat used in this study had reached an advanced stage of oxidation and had a low amount of readily oxidizable material left. Lastly, it seems that the tailings utilized available DO in the water covers at a rate exceeding the diffusion of oxygen from the atmosphere into the circulated water cover. Overall, the oxygen fluxes based on dissolved oxygen values measured after 18 months and calculated from Fick's equations were very low: the lowest was the peat layer ($3.8 \text{ gO}_2 \text{ m}^{-2} \text{ year}^{-1}$) and the highest was the 1 meter water cover ($6.3 \text{ gO}_2 \text{ m}^{-2} \text{ year}^{-1}$). The smaller flux into the peat layer reflects a deeper oxygen penetration and possibly a slower oxygen diffusion rate.

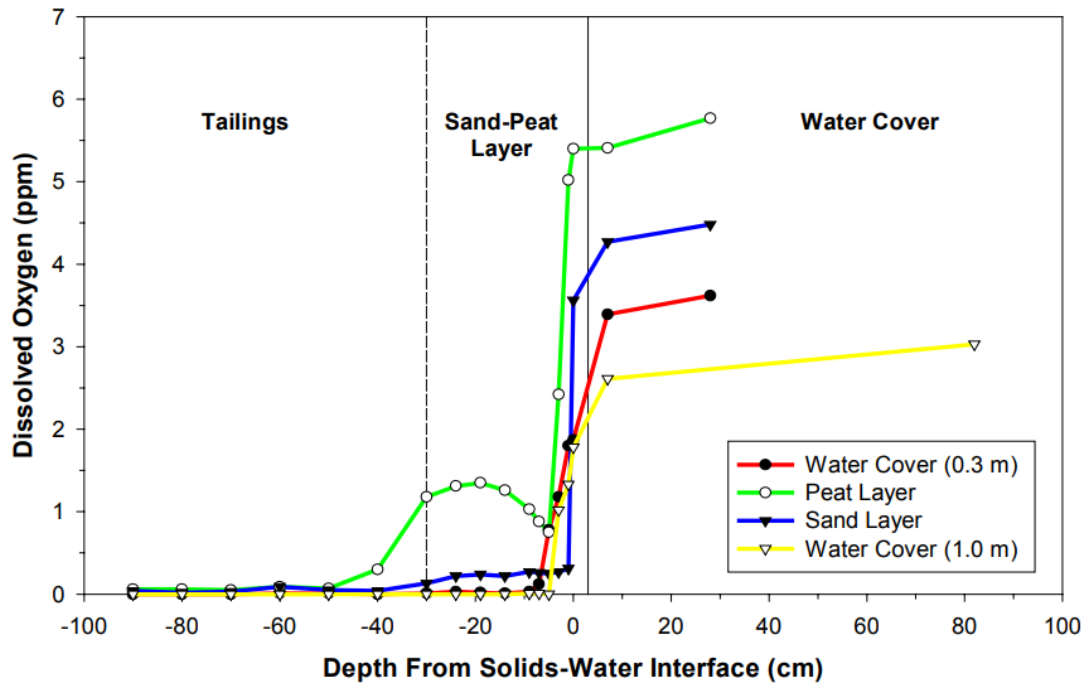


Figure 4: Dissolved Oxygen (mg/L) profiles, day 100 (from MEND, 2001)

Li and Catalan (1997) conducted a numerical study with Soil Cover software in order to compare the results that could be expected with a cover of low-sulphide tailings (0.1 wt.% - 0.3 wt.% sulphide) combined with a very low water table of four meters below surface, versus an aqueous cover. From those results, in order to reduce the flux to 50 times less than the reference scenario (no cover), a 2.5 m cover of desulphurized tailings (0.1% sulphide) would be necessary, while to obtain similar results using an aqueous cover, the thickness would need to be about 3.5 m.

Overall, these results confirm that a monolayer cover consisting of low-sulphide tailings with water level control (elevated water table) could successfully reduce oxygen uptake into the cover and ultimately limit AMD generation, at least at room temperature.

3.1 Frozen Partially Saturated Porous Media

Although gas migration and oxidation reactions are significantly reduced in frozen materials, several authors argue that neglecting oxygen fluxes when the ground is frozen tends to cause an underestimation of the oxygen fluxes that reach the reactive waste (Davé et al., 2017; MEND, 2006). Elberling (2005) has shown that even at a temperature of -11°C , oxygen consumption and migration can occur. As mentioned prior, the MEND 1.61.6 report highlights a need for the investigation of the effect of below freezing temperatures on oxygen migration phenomena (MEND, 2006).

Several changes in the physical and chemical characteristics of water and air present in the pores of the soil accompany freezing temperatures, subsequently complicating the fluid dynamics and diffusion of gases. Indeed, below 0°C a portion of the water freezes while water retained by capillarity or located in very fine pores does not freeze (Spaans & Baker, 1996). This can also be accompanied by swelling of the sample when pore space is not sufficient to accommodate the increased volume due to expansion of the interstitial water. In addition to swelling, oxygen diffusion may be impacted by partial or total freezing, in particular the D_e and K_r .

3.1.1 Estimation of the diffusion coefficient in partially saturated and frozen porous media

As discussed in Section 2.1, for ambient temperatures, D_e can be estimated from different empirical and semi-empirical predictive models. Among the models that consider diffusion in the gaseous and liquid phase is the model of Aachib et al. (2004), which can be written as:

$$D_e = \frac{1}{n^2} (D_a^0 \theta_a^{p_a} + H D_w^0 \theta_w^{p_w}) \quad (\text{Equation 5})$$

Where n represents the porosity of the material, D_i^0 represents the coefficient of free diffusion of oxygen in water (D_w^0) or air (D_a^0), H is Henry's constant and p_a and p_w are obtained as a function of the volumetric air (θ_a) and water (θ_w), content as:

$$p_a = 1.201\theta_a^3 - 1.515\theta_a^2 + 0.987\theta_a + 3.118 \quad (\text{Equation 6})$$

$$p_w = 1.201\theta_w^3 - 1.515\theta_w^2 + 0.987\theta_w + 3.118 \quad (\text{Equation 7})$$

Through these equations, several parameters will directly influence the calculated flux. Furthermore, many of those parameters will be strongly influenced by a change in temperature and/or freezing. This is particularly the case for porosity, which could undergo a variation of its value following freezing if the volume of expansion of water is greater than the volume of air available in the porous material before frost (swelling phenomenon).

The free diffusion coefficient of oxygen in water and in air must also be adapted to the new temperatures. Following the relation of Denny (1993):

$$D_a^0(T) = k_1 T^{k_2} \quad (\text{Equation 8})$$

Where T represents the temperature in Kelvin and k_1 and k_2 are coefficients that vary from one molecule to another.

The free diffusion coefficient in water D_w^0 can be estimated with the equation of Richards (1969), as:

$$D_w^0(T) = \frac{7.4 \cdot 10^{-8} \cdot T (\psi_{H_2O} M_{H_2O})^{\frac{1}{2}}}{\mu V_{O_2}^{0.6}} \quad (\text{Equation 9})$$

Where T is the temperature in Kelvin, ψ_{H_2O} is a parameter equal to 2.25 according to Reid et al. (1977), M_{H_2O} is the molecular weight of water (18 g/mol), μ is the dynamic viscosity of water in mPa-s (temperature-dependent variable, can be calculated according to the Kestin et al. equation (1978)) and V_{O_2} is the molecular volume of oxygen (25.6 cm³/ g-mole).

Determination of Henry's constant for temperatures below 0° C can be done using Sander's formula (2015) and using data from Sander et al. (2006).

The volumetric water and air contents must also be replaced by the unfrozen volumetric water content (UVWC or θ_{w-f}) and the frozen volumetric air content (FVAC or θ_{a-f}). The UVWC values can be measured with probes while the FVAC values can be deduced from the final porosity of the material, such as:

$$n_f = \theta_{a-f} + \theta_{w-f} \quad (\text{Equation 10})$$

It should be noted, however, that Equation 10 is only valid when the degree of saturation of the solid material is less than 91.7%, i.e., when the volume of expansion of water is greater than the volume of air available in the porous material before frost (Nyameogo, 2017).

Overall, the adaptation of Aachib's equation (Equation 5) for freezing temperature in partially saturated ($S_r < 91,7\%$) porous media leads to:

$$D_{e-frozen} = \frac{1}{n_f^2} (D_a^0(T) \theta_{a-f}^{p_a} + H(T) D_w^0(T) \theta_{w-f}^{p_w}) \quad (\text{Equation 11})$$

However, as Nyameogo (2017) points out, the equations defining the parameters p_a and p_w have been developed empirically and at ambient temperature (20° C), hence the interest in adapting the traditional diffusion-consumption tests for sub-zero temperatures.

To remedy this knowledge gap, Nyameogo (2017) adapted the traditional double chamber cell test for the determination of D_e for freezing temperatures. According to the experimental values obtained, it seems that even by adjusting the parameters of Equation 4 as a function of the test temperature, the predictive model would slightly overestimate the real value of D_e , which would then lead to an overestimation of the oxygen fluxes. This result was expected since, as described in Section 3.1.1 the equations that predict the values of p_a and p_w (dependent on the tortuosity) do not consider freezing temperatures. According to Nyameogo (2017), no further studies have been conducted comparing calculated versus measured D_e values for temperatures below 0°C.

3.1.2 Estimation of the reaction rate coefficient in partially saturated and frozen porous media

In a similar way to D_e , K_r must also be adapted to frozen conditions. However, unlike D_e , a relationship linking K_r and temperature has already been identified in the literature and corresponds to the adapted Arrhenius equation (Nicholson et al., 1988):

$$\ln \frac{K_{r1}}{K_{r2}} = E_a \frac{(T_1 - T_2)}{RT_1 T_2} \quad (\text{Equation 12})$$

In this equation, K_{r1} and K_{r2} correspond to the reaction rates at temperatures (in Kelvin) T_1 and T_2 , E_a is the activation energy (variable depending on the sulphurous ores present in the material) and R is the universal gas constant ($8.314 \cdot 10^{-3} \text{ kJ mol}^{-1} \text{ K}^{-1}$). According to Coulombe (2012), who investigated the effect of temperature on the flux of oxygen, predictions based on the Arrhenius equation would yield results very similar to those obtained experimentally, even for temperatures down to -8°C . However, as shown in Figure 5, the value of the chosen activation energy will have a significant impact on the accuracy of the results. Nyameogo (2017) came to similar conclusions using an adapted double-chamber test.

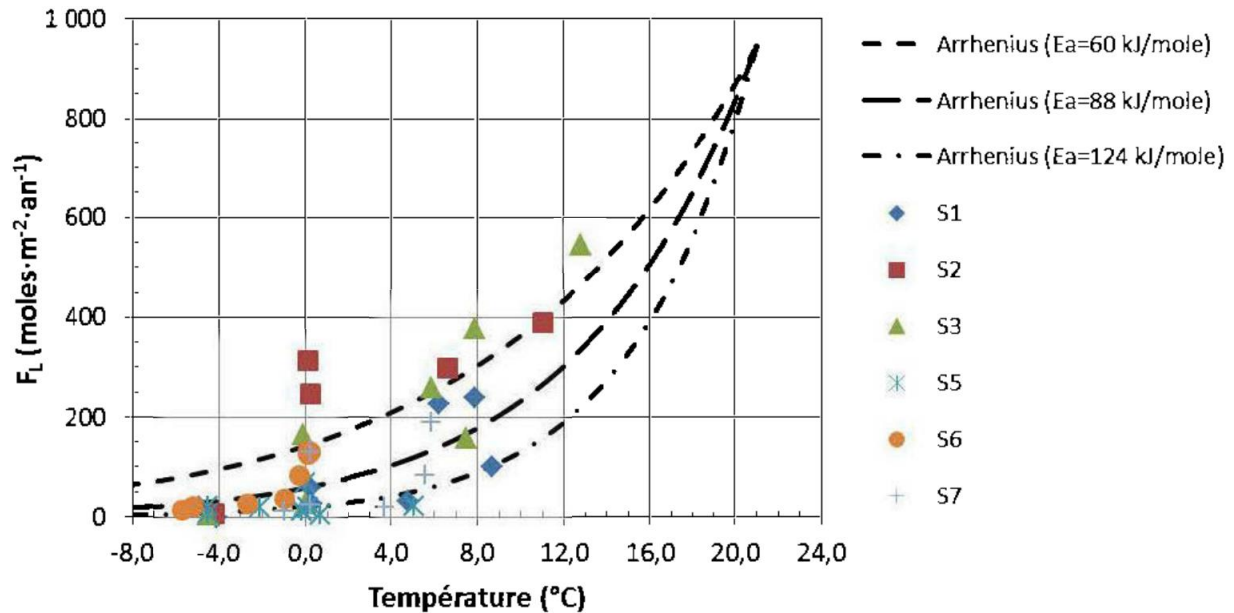


Figure 5: Effect of temperature on the flux of oxygen (Coulombe, 2012)

4 Experimental Design

Very little research has been done to investigate the impact of the freezing phenomenon on oxygen migration within saturated covers. Therefore, there is a need to further understand oxygen diffusion dynamics in these particular conditions in order to estimate the oxygen flux that can reach reactive tailings during cold winter months, under freezing conditions. The experimental design focused on oxygen concentration and unfrozen volumetric water content within freezing conditions through a series of laboratory column experiments.

4.1 Objectives

The objectives of the proposed experiments were:

1. For various water table levels, determine how the unfrozen volumetric water content (UVWC) in the saturated and unsaturated portions of an inert cover material will evolve according to depth under freezing conditions (-8°C);

2. Predict the oxygen profiles in the low-level water column and the mid-level water columns in conjunction with changes in temperature.

4.2 Material and Methods

The simplest method to determine oxygen flux through a material is to use the gradient method and apply Fick's first law of diffusion (Section 2.3.2). However, when working with sub-zero temperatures, this method became hard to use, especially when it came to the oxygen measurement. O₂ optic sensors typically will not work properly under 0°C and gas chromatography can be very expensive. Often designed for use in soil applications, galvanic cell sensors equipped with a thermistor temperature sensor to correct for temperature changes (up to -20°C) appeared to be a suitable compromise between price and functionality. However, galvanic cell sensors tend to consume a certain amount of oxygen per day (2.2 μmol O₂/day) due to the electrochemical reaction of oxygen with the electrolyte present in the sensor. Thus, to obtain precise concentration results, the time needed to perform the experiments has to be as short as possible. They can also only work in partially water-saturated media.

To overcome these issues and to be able to predict the results for multiple field scenarios, it was decided that the oxygen fluxes in the fully water-saturated portion would be determined by modeling. In order to create a representative model of freezing conditions for the numerical simulations, laboratory scale instrumented columns were constructed, and the following parameters were monitored over time and depth:

- Volumetric water content;
- Unfrozen volumetric water content (UVWC);
- Temperature; and
- Oxygen concentration gradient between the water interface and the top of the cover material (only the partially water-saturated portion).

4.2.1 Cover material

The inert material chosen for this study was a mixture of dry sand (50%) and a silty silica powder (50%) in order to reach a granulometry that was not too fine or too coarse, similar to that of tailings. To determine the particle-size distribution, a series of square mesh sieves were used and the relative density of the grains (D_r) was determined with a helium pycnometer.

4.2.2 Column set-up

The cylindrical columns used for this study had a total height of 40" and an internal diameter of 3". Each column was constructed using two 12" Acrylonitrile-Butadiene-Styrene (ABS) pipe sections and one 16" ABS pipe section, joined by couplings, to facilitate the construction and maintenance of the experiment setup. ABS pipe was chosen over Polyvinyl Chloride (PVC), as ABS is more resistant to internal pressure changes that could result from expanding pore water during freezing conditions.

The tops of the columns were open to the atmosphere to allow for oxygen to diffuse into the cover material. At the bottom of each column, an outflow port was connected to a container by tubing. This container was maintained at a height equal to the desired water table level for the column. This allowed water to flow into

the container and maintain a water table level within the column via hydrostatic equilibrium. The experimental setup is shown in Figure 6.

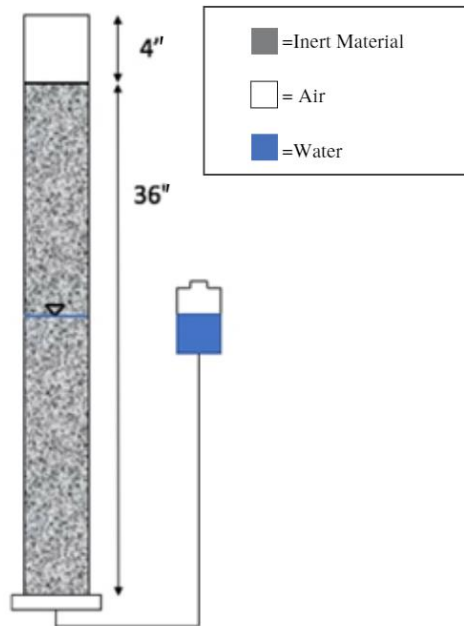


Figure 6: Experimental setup

4.2.3 Parameter monitoring

In order to properly construct the models as well as to fulfill the first objective, measurement of the volumetric water content and temperature were conducted using four 5TM probes (Decagon Devices, Inc.) evenly installed across depth (Figure 7).

It was also decided that oxygen concentration values would be examined in order to further analyze the relationship between UVWC, temperature and oxygen concentration. Thus, two galvanic cell O_2 sensors (SO-110, Apogee Instrument Inc.) equipped with diffusion head (to keep the soil and debris clear of the sensor and ensure accurate measurements) were installed in the partially saturated portion of the cover. Since this type of sensor only measures the gaseous O_2 concentration, one of them was placed approximately 2 cm below the surface of the cover material while the other was placed 2 cm above the water interface (Figure 7). UVWC data was collected every minute using a 6 channel datalogger (ZL6, Meter Environment), and oxygen concentration data was collected when equilibrium was fully reached. Since the material used for the cover was relatively coarse, it was estimated that this equilibrium should be reached in a relatively short amount of time. Multiple measurements were taken over time to ensure the validity of this hypothesis.

Since the 5TM probes chosen for the measurement of UVWC in the cover material had the potential to, by their size, hamper the diffusion of oxygen, two different columns were used for each parameter: one for the UVWC and one for oxygen gradient measurement (Figure 7).

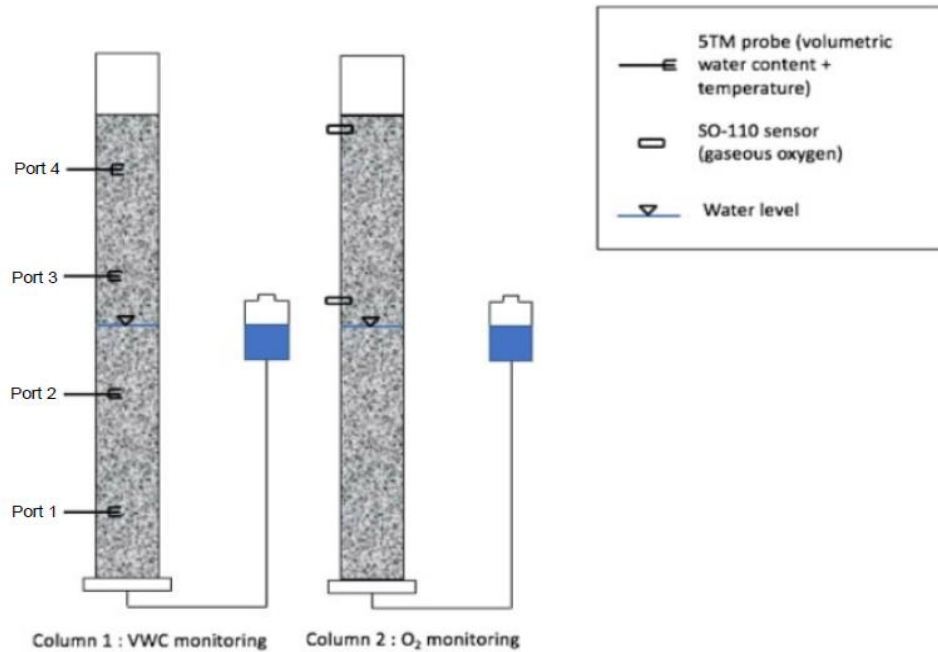


Figure 7: Instrumented columns

4.3 Experimental Protocol

Initially, 1 L of water was added to columns 1 and 2 and allowed to percolate through the materials to the bottom of each column and into the hydrostatic equilibrium container. Once the desired water table level was acquired for each column, confirmed by the hydrostatic equilibrium container and by sight, any additional water over and above the amount necessary to maintain the desired water-table level was siphoned out via an additional outflow tube at the bottom of the column, equipped with a valve to avoid oxygen penetration into the base of the column via this outflow.

After reaching the desired water table level, the columns were placed in a freezer maintained at -8°C , until stabilization of the UVWC and O_2 concentration values (O_2 values will never be fully stable due to the consumption of oxygen by the probes). Then, the columns were taken out of the freezer to room temperature until new and stable values of UVWC and O_2 concentration were obtained. The three water tables scenarios that were investigated are presented in Figure 8.

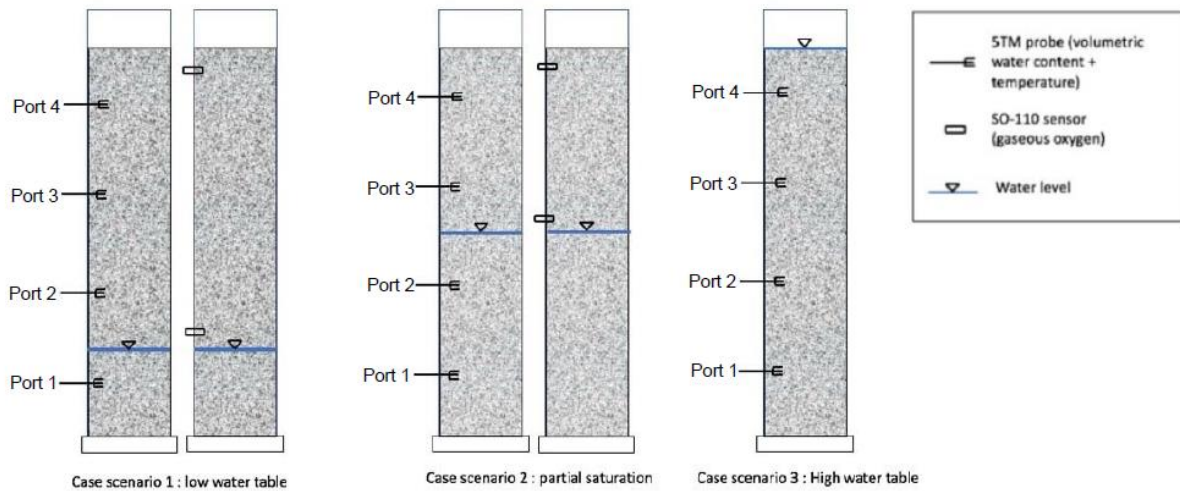


Figure 8: Case scenario involving different water table height

5 Interpretation of the Results

5.1 Data Analysis and Unfrozen Volumetric Water Content

Three different laboratory column experiments were conducted: Case Scenario 1: low water table (bottom); Case Scenario 2: partial saturation (middle); and Case Scenario 3: high water table (top). Each of the columns began at room temperature and then were cooled until frozen before going back up to room temperature. 5TM probes (Decagon Devices, Inc) were utilized to measure the volumetric water content and soil temperature. The results for each Case Scenario are summarized below.

5.1.1 Case Scenario 1 - Low Water Level

In Port 1 illustrated in Figure 9, which was submerged, as temperature was decreased from room temperature ($\sim 22^{\circ}\text{C}$), UVWC remained relatively stable at $0.28 \text{ m}^3/\text{m}^3$ until the temperature reached approximately -1.5°C (Figure 9). When temperature was lowered past -1.7°C , the UVWC decreased to $0.05 \text{ m}^3/\text{m}^3$ (Figure 9).

Conversely, during the thawing process, the UVWC did not increase from $0.05 \text{ m}^3/\text{m}^3$ until the temperature reached 1.7°C , at which point it increased to approximately the same UVWC as the initial measurement ($0.30 \text{ m}^3/\text{m}^3$) and remained at this UVWC until the temperature returned to room temperature (Figure 9).

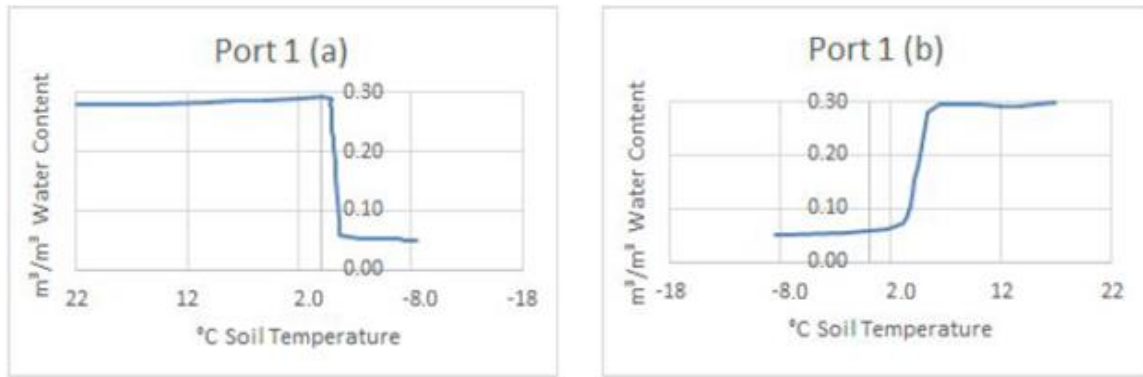


Figure 9: Case Scenario 1 - water content measured at Port 1 (submerged) during (a) freeze & (b) thaw

In Port 2 (Figure 10), which was not submerged, as the columns went through the freeze cycle, UVWC was relatively constant $\sim 0.20 \text{ m}^3/\text{m}^3$ as the temperature was reduced from room temperature to around -1.1°C (Figure 10), the UVWC was stable. However, the UVWC decreased almost immediately in the submerged Port 1 when temperatures reached -1.7°C , in the unsubmerged Port 2, the UVWC briefly stabilized around $0.10 \text{ m}^3/\text{m}^3$ at temperatures from -1.1°C until -1.9°C . Then, after reaching a temperature of -1.9°C , there was an almost immediate decrease in UVWC from $0.10 \text{ m}^3/\text{m}^3$ to $0.044 \text{ m}^3/\text{m}^3$ (Figure 10).

As the columns were thawed, UVWC remained at $0.044 \text{ m}^3/\text{m}^3$ until the temperature was raised to 2.5°C . At 2.6°C UVWC increased sharply to $\sim 0.24 \text{ m}^3/\text{m}^3$, where it stabilized for the duration of the experiment. There was a slight and short-lived increase in UVWC from $0.24 \text{ m}^3/\text{m}^3$ to $0.25 \text{ m}^3/\text{m}^3$ when the temperature went from 5.0°C to 5.7°C . However, by 7.2°C , UVWC was back to $0.24 \text{ m}^3/\text{m}^3$ (Figure 10). See Figure 11, for more details.

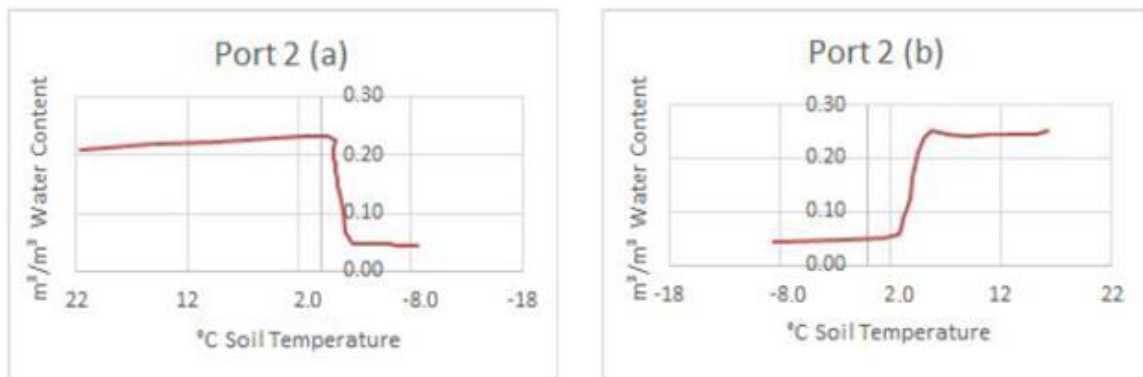


Figure 10: Case Scenario 1 - water content measured at Port 2 (un-submerged) during (a) freeze & (b) thaw

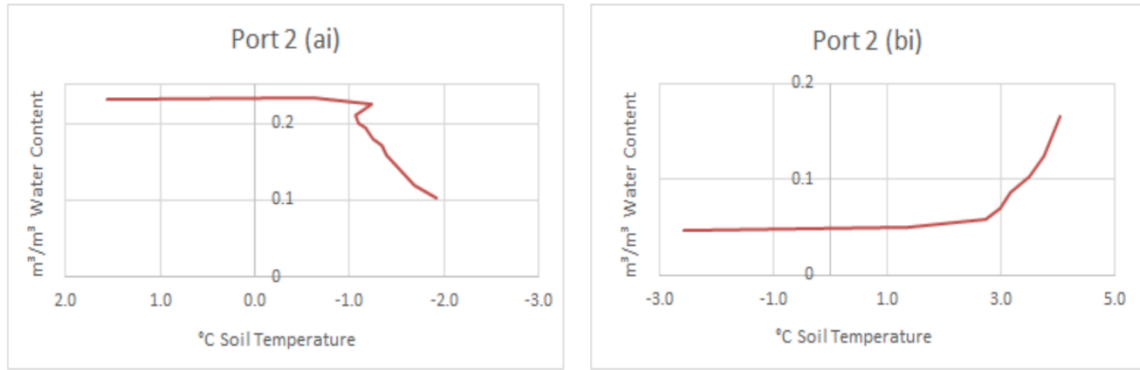


Figure 11: Case Scenario 1 – water content measured at Port 2 (unsubmerged) during (ai) freeze & (bi) thaw, with a focus on the unfrozen water level increase and decrease

The trajectory of the freeze cycle taking place around Port 3 (Figure 12) strongly resembled the results in Port 1 and Port 2, with a single decreasing step in UVWC occurring at -1.3°C (Figure 12). However, the range of UVWC during the freeze cycle was much smaller. Where the UVWC ranged from $0.05\text{ m}^3/\text{m}^3$ to $0.3\text{ m}^3/\text{m}^3$ in Port 1 (i.e., 0.25 difference), and from $0.044\text{ m}^3/\text{m}^3$ to $0.2\text{ m}^3/\text{m}^3$ in Port 2 (i.e., 0.16 difference), in Port 3, the UVWC ranged only from $0.05\text{ m}^3/\text{m}^3$ to the limit of quantification ($<0.02\text{ m}^3/\text{m}^3$) equivalent to a 0.03 change (Figure 12).

During the thaw cycle, there was a wider range of UVWC, more similar to Ports 1 and 2. However, the steps in UVWC occurred in 3 smaller steps, as opposed to one large step which occurred in Ports 1 and 2. The first step occurred at 1.8°C from the limit of quantification ($<0.02\text{ m}^3/\text{m}^3$) to $0.015\text{ m}^3/\text{m}^3$. The UVWC was then relatively stable from 1.8°C to 13°C , when UVWC increased sharply to $0.17\text{ m}^3/\text{m}^3$. At room temperature, UVWC spiked again to $0.26\text{ m}^3/\text{m}^3$ (Figure 12).

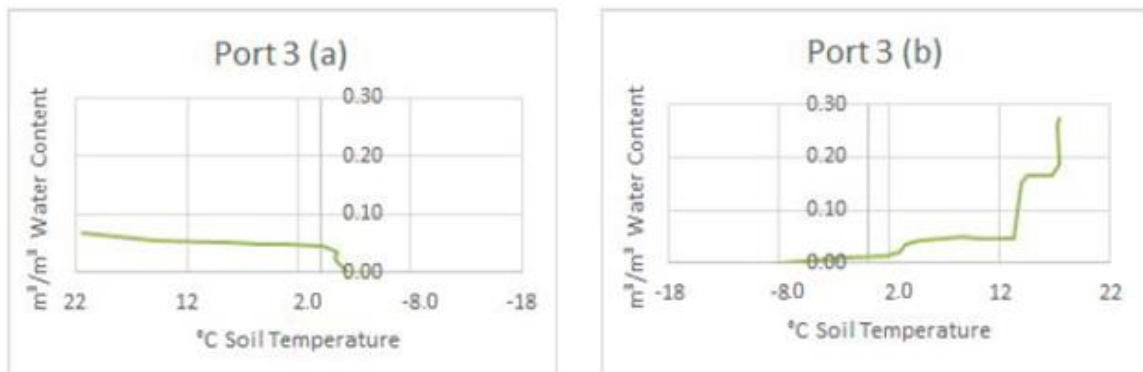


Figure 12: Case Scenario 1 - water content measured at Port 3 (un-submerged) during (a) freeze & (b) thaw

As indicated by figure 13 port 4 froze and thawed in similar patterns to Ports 1 and 2 (i.e., in a single decreasing step), the overall range in UVWC was again lower than that in Port 3 – i.e., ranged from only below the detection limit to $0.028\text{ m}^3/\text{m}^3$ (a range of only $0.023\text{ m}^3/\text{m}^3$ - Figure 13). The decreasing step occurred at a similar temperature as Ports 1, 2 and 3 – around -0.80°C . After this point there is a steady decline in the unfrozen volumetric water content, until it declined to a value below limit detection

During the thaw cycle, the increase in UVWC was a more gradual increase, with an increase in UVWC from below the detection limit to $0.025\text{m}^3/\text{m}^3$ as the temperature increased from -1.6°C to 6.8°C . The UVWC stabilized at around $0.025\text{m}^3/\text{m}^3$ at temperatures above 6.8°C (Figure 13).

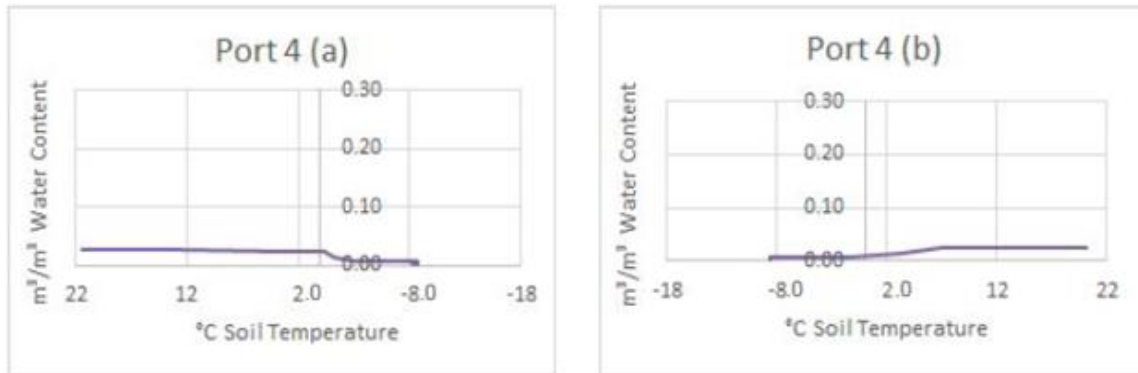


Figure 13: Case Scenario 1 - water content measured at Port 4 (un-submerged) during (a) freeze & (b) thaw

Overall, it appeared that the range of UVWC decreased with distance from the water level (i.e., overall UVWC in Port 1 > Port 2 > Port 3 > Port 4). This was expected, as the water level for in Case Scenario 1 was closer to the bottom of the column, between Port 1 and 2, and due to the fact that there is a larger quantity of UVWC at the base of the column, than at the surface.

Despite the differences in overall UVWC ranges, the temperature at which the UVWC shifted were relatively consistent between ports – at between -1.5°C and -0.2°C for the freeze cycle and 3°C and 2.8°C for the thaw cycle. Upon reaching this value there was a steep decline (freeze) or incline (thaw) in the UVWC value for a few degrees before UVWC re-stabilized.

Freeze and thaw seemed to mirror each other in the way they both had regions of stability in UVWC as temperature increased or decreased, followed by a fairly steep drop in UVWC - which seemed to decrease in the quantity by which it declined as the ports moved further from the water level, finished by another region of stability.

Regardless of the port or the temperature, following the drop in UVWC, there was still unfrozen water present throughout the entire column. At the coldest point, the remaining UVWC at each port was:

- Port 1: $0.053\text{m}^3/\text{m}^3$
- Port 2: $0.044\text{m}^3/\text{m}^3$
- Port 3: Below detection limit
- Port 4: Below detection limit

5.1.2 Case Scenario 2 - Mid Water Level

From room temperature to -0.60°C (Figure 14), the UVWC remained steady at $0.27\text{m}^3/\text{m}^3$, until reaching a temperature of -0.60°C . At that point, there seemed to be a decline starting when the temperature went from -0.60°C with a UVWC of $0.29\text{m}^3/\text{m}^3$ to -2.6°C with a UVWC of $0.26\text{m}^3/\text{m}^3$, down to -2.1°C with a UVWC of $0.19\text{m}^3/\text{m}^3$ (i.e., a decline of $0.10\text{m}^3/\text{m}^3$). After reaching a temperature of -2.1°C , the UVWC

decreased down to $0.056 \text{ m}^3/\text{m}^3$ in the span of 3.8°C before leveling out around $0.055 \text{ m}^3/\text{m}^3$ for the remainder of the freeze cycle.

From the freeze point to 1.8°C , the UVWC was maintained around $0.061 \text{ m}^3/\text{m}^3$, before a steep incline to $0.28 \text{ m}^3/\text{m}^3$ at 6.1°C , where it maintained a UVWC around $0.28 \text{ m}^3/\text{m}^3$ for the rest of the cycle.

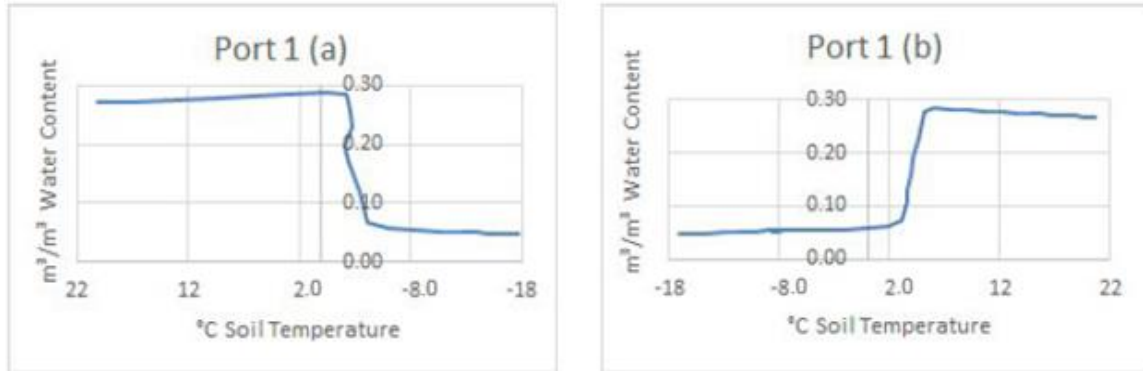


Figure 14: Case Scenario 2 - water content measured at Port 1 (submerged) during (a) freeze & (b) thaw

From room temperature to -1.1°C (Figure 15), the UVWC stayed at a UVWC of around $0.25 \text{ m}^3/\text{m}^3$. The UVWC then dropped $0.19 \text{ m}^3/\text{m}^3$ in the span of 5.2°C . $0.69 \text{ m}^3/\text{m}^3$ into the drop, there seemed to be a bump, where the temperature went from -3.1°C at a UVWC of $0.18 \text{ m}^3/\text{m}^3$, up to -2.4°C with a UVWC of $0.16 \text{ m}^3/\text{m}^3$ and then back down to -3.8°C with a UVWC of $0.13 \text{ m}^3/\text{m}^3$. Following the drop, the UVWC leveled out around $0.030 \text{ m}^3/\text{m}^3$ for the remaining freeze cycle.

From the freeze point to 1.6°C , the UVWC was maintained around $0.44 \text{ m}^3/\text{m}^3$, before drastically increasing to $0.25 \text{ m}^3/\text{m}^3$ at 5.8°C and maintaining a UVWC around $0.24 \text{ m}^3/\text{m}^3$ for the rest of the cycle.

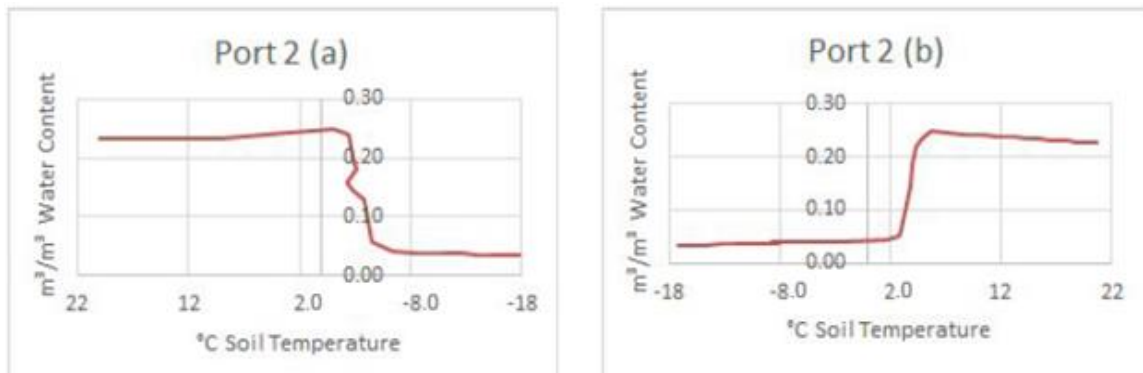


Figure 15: Case Scenario 2 - water content measured at Port 2 (submerged) during (a) freeze & (b) thaw

As illustrated by Figure 16, from room temperature to -2.8°C , the UVWC stayed steady around $0.24 \text{ m}^3/\text{m}^3$. The UVWC then dropped $0.15 \text{ m}^3/\text{m}^3$ in the span of 2.5°C . $0.182 \text{ m}^3/\text{m}^3$ into the drop, there is a bump, where the temperature went from -3°C with a UVWC of $0.18 \text{ m}^3/\text{m}^3$, up to -1.9°C with a UVWC of 0.16

m^3/m^3 , back down to -3.1°C with a UVWC of $0.087 \text{ m}^3/\text{m}^3$, before continuing its decline. Upon reaching a temperature of -5.5°C , the UVWC leveled out around $0.045 \text{ m}^3/\text{m}^3$ for the remaining freeze cycle.

From the freeze point to 0.9°C , the UVWC was maintained around $0.045 \text{ m}^3/\text{m}^3$, before drastically increasing to $0.21 \text{ m}^3/\text{m}^3$ at 6.2°C and maintaining a UVWC around $0.21 \text{ m}^3/\text{m}^3$ for the rest of the cycle.

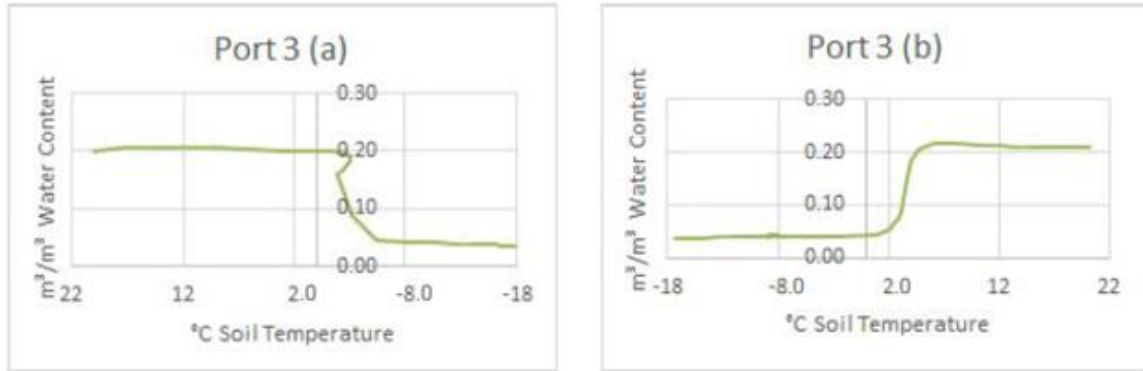


Figure 16: Case Scenario 2 - water content measured at Port 3 (un-submerged) during (a) freeze & (b) thaw

Figure 17 shows that from room temperature to -2.8°C , the UVWC stays around $0.017 \text{ m}^3/\text{m}^3$. Upon reaching -2.8°C , the UVWC plummeted to $0.001 \text{ m}^3/\text{m}^3$, at -7.4°C , before leveling out around $0.001 \text{ m}^3/\text{m}^3$ for the remainder of the freeze.

From the freeze point to -7.4°C , the UVWC was maintained around $0.001 \text{ m}^3/\text{m}^3$, before it increased to $0.017 \text{ m}^3/\text{m}^3$ at -2.8°C and maintained a UVWC below the detection limit until reaching the coldest temperature.

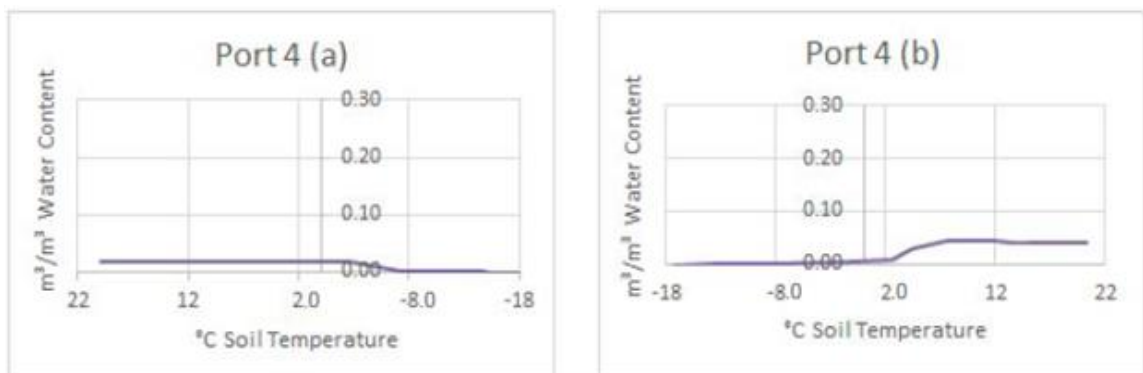


Figure 17: Case Scenario 2 - water content measured at Port 4 (un-submerged) during (a) freeze & (b) thaw

The UVWC per port tended to stay at a steady value until reaching a temperature between -2.0°C and -6.3°C for freeze and 2°C and 3°C for thaw. Upon reaching this value there was a steep decline (freeze) or incline (thaw) in the UVWC value for a few degrees before leveling out again. Similar to the low water level the UVWC per port moving away from the water level decreased. The UVWC for port 1 started with a UVWC of $0.27 \text{ m}^3/\text{m}^3$ and ended at $0.28 \text{ m}^3/\text{m}^3$. Port 2 started at a UVWC of $0.25 \text{ m}^3/\text{m}^3$ and ended at

0.24 m³/m³. Port 3 started at a UVWC of 0.24 m³/m³ and ended at 0.21 m³/m³. Port 4 started 0.017 m³/m³ and ended at 0.025 m³/m³. It appeared the UVWC tended to increase or decrease by 0.014 m³/m³ to 0.04 m³/m³ to 0.017 m³/m³. The fact that the UVWC decreased, as the port number increased was expected, as the water level for this case scenario was closer to the middle, as well as the fact that there is a higher quantity of UVWC at the base of the column, than at the surface.

Freeze and thaw seemed to mirror each other in the way they both had regions of stability in UVWC as temperature increased or decreased, followed by a fairly steep drop in temperature — which seems to decrease in the quantity by which it declines as the ports move further from the water level, finished by another region of stability.

For this water level the UVWC for each port at the coldest point was:

- Port 1: 0.050 m³/m³
- Port 2: 0.030 m³/m³
- Port 3: 0.040 m³/m³
- Port 4: Below detection limit

Regardless of the port or the temperature, following the drop in UVWC, there was still unfrozen water present throughout the entire column. At the coldest point, the remaining UVWC at each port was at mid-level water.

5.1.3 Case scenario 3: High Water Level (Above port 4)

From room temperature to 0.90°C (figure 18), the UVWC was maintained around 0.28 m³/m³, before it drastically declined to 0.061 m³/m³ at -1.9°C and maintained a UVWC around 0.060 m³/m³ until it reached the freeze point.

From freeze to 2.4°C, the UVWC was maintained around 0.062 m³/m³, before it drastically increased to 0.29 m³/m³ at 5.5°C, and then maintained a UVWC around 0.28 m³/m³ until reaching room temperature again.

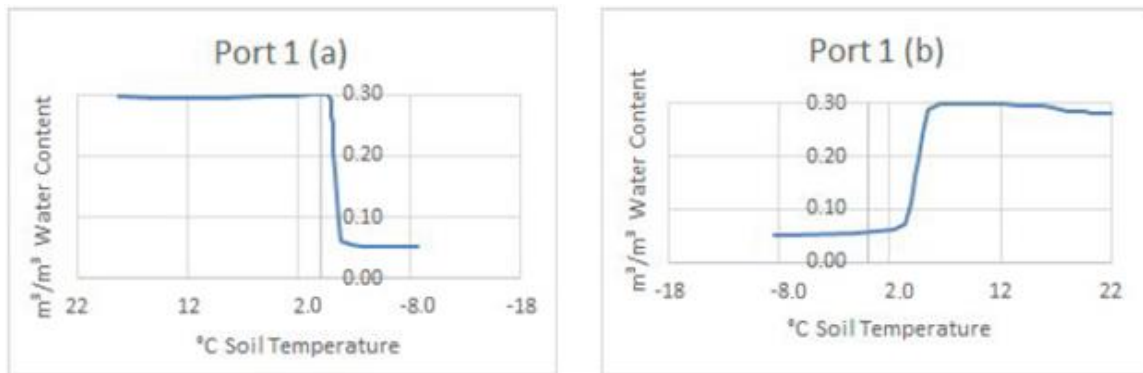


Figure18: Case Scenario 3 - water content measured at Port 1 (submerged) during (a) freeze & (b) thaw

From room temperature to -0.80°C (Figure 19), the UVWC was maintained around $0.24 \text{ m}^3/\text{m}^3$, before drastically declining to $0.053 \text{ m}^3/\text{m}^3$ at -2.4°C and maintaining a UVWC around $0.050 \text{ m}^3/\text{m}^3$ until reaching the freeze point. From the freeze point to 2.9°C , the UVWC was maintained around $0.060 \text{ m}^3/\text{m}^3$, before drastically increasing to $0.25 \text{ m}^3/\text{m}^3$ at 5.6°C , and then maintaining a UVWC around $0.24 \text{ m}^3/\text{m}^3$ until reaching room temperature again.

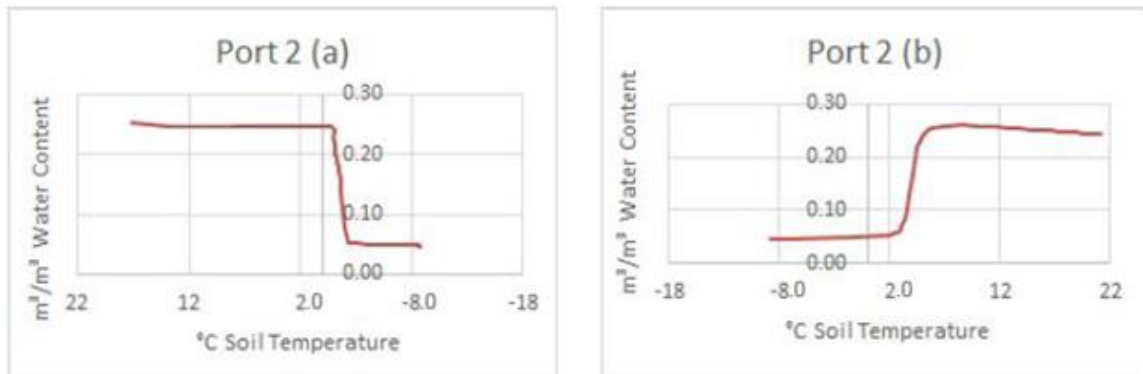


Figure 19: Case Scenario 3 - water content measured at Port 2 (submerged) during (a) freeze & (b) thaw

From room temperature to -0.20°C (Figure 20), the UVWC was maintained around $0.25 \text{ m}^3/\text{m}^3$, before it drastically declined to $0.015 \text{ m}^3/\text{m}^3$ at -2.4°C and maintained a UVWC of around $0.010 \text{ m}^3/\text{m}^3$ until it reached the freeze point. Prior to the decline, there seemed to be a small bump, where the temperature went from -0.20°C with a UVWC of $0.25 \text{ m}^3/\text{m}^3$ to -1.2°C with a UVWC of $0.25 \text{ m}^3/\text{m}^3$, back up to -0.90°C with a UVWC of $0.24 \text{ m}^3/\text{m}^3$.

From the freeze point to 2.5°C , the UVWC increased $0.030 \text{ m}^3/\text{m}^3$, before it drastically increased to a UVWC of $0.28 \text{ m}^3/\text{m}^3$ at 6.0°C , and then maintaining a UVWC $0.27 \text{ m}^3/\text{m}^3$ until reaching room temperature again.



Figure 20: Case Scenario 3 - water content measured at Port 3 (submerged) during (a) freeze & (b) thaw

This port (Figure 21) did not seem to look like any of the others in this or any of the other water levels. It began at room temperature with a UVWC of $0.072 \text{ m}^3/\text{m}^3$, it then sloped up to $0.13 \text{ m}^3/\text{m}^3$ at 16°C , and then to $0.13 \text{ m}^3/\text{m}^3$ at 7.6°C , before it declined to $0.091 \text{ m}^3/\text{m}^3$ at -0.10°C , and declined down to $0.042 \text{ m}^3/\text{m}^3$ until -8.0°C .

The thaw for this specific port is rather unique. It begins with a UVWC of $0.042 \text{ m}^3/\text{m}^3$ at -8.1°C , and maintains a UVWC between $0.042 \text{ m}^3/\text{m}^3$ and $0.055 \text{ m}^3/\text{m}^3$ until 2.1°C , where it goes from $0.055 \text{ m}^3/\text{m}^3$, up to $0.097 \text{ m}^3/\text{m}^3$ at 4.4°C , before sloping down to $0.069 \text{ m}^3/\text{m}^3$ at 14°C . From here, it increases to $0.17 \text{ m}^3/\text{m}^3$ at 15°C and maintaining a value around that until reaching room temperature.

Similar to the previous water levels the UVWC per port moving away from the water level decreased. The UVWC per port tended to stay at a steady value until it reached a temperature between -1.9°C and -4.3°C for freeze and 2.0°C and 3.0°C for thaw. Upon reaching this value there was a steep decline (freeze) or incline (thaw) in the UVWC value for a few degrees before leveling out again. The UVWC for port 1 started with a UVWC of $0.28 \text{ m}^3/\text{m}^3$ and ended at $0.28 \text{ m}^3/\text{m}^3$. Port 2 started at a UVWC of $0.24 \text{ m}^3/\text{m}^3$ and ended at $0.24 \text{ m}^3/\text{m}^3$. Port 3 started at a UVWC of $0.25 \text{ m}^3/\text{m}^3$ and ended at $0.27 \text{ m}^3/\text{m}^3$. Port 4 started $0.072 \text{ m}^3/\text{m}^3$ and ended at $0.17 \text{ m}^3/\text{m}^3$. It appears the UVWC tended to increase or decrease by 0.02 to $0.05 \text{ m}^3/\text{m}^3$ to $0.017 \text{ m}^3/\text{m}^3$. The fact that the UVWC decreased, as the port number increased was expected, as the water level for this case scenario was closer to the middle, as well as the fact that there was a higher quantity of UVWC at the base of the column, than at the surface.

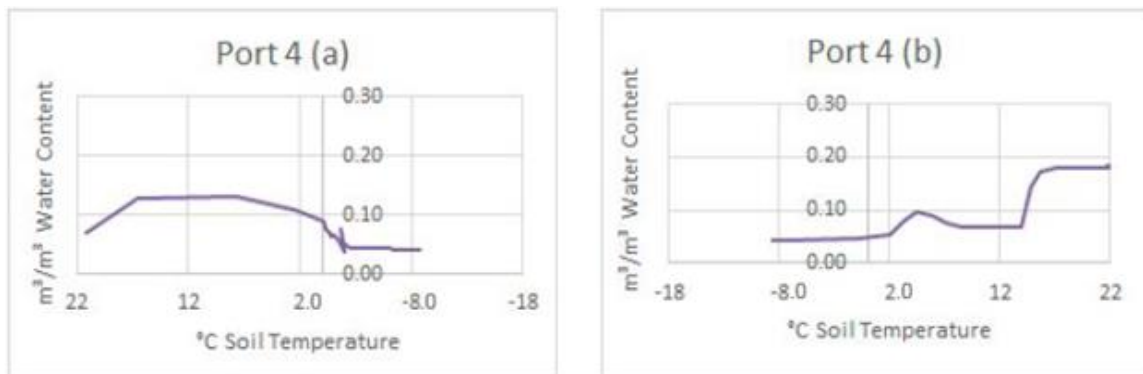


Figure 21: Case Scenario 3 - water content measured at Port 4 (submerged) during (a) freeze & (b) thaw

Freeze and thaw seemed to mirror each other in the way they both had regions of stability in UVWC as temperature increased or decreased, followed by a fairly steep drop in temperature — which seemed to decrease in the quantity by which it declined as the ports move further from the water level, finished by another region of stability.

For this water level the UVWC for each port at the coldest point was:

- Port 1: $0.050 \text{ m}^3/\text{m}^3$
- Port 2: $0.048 \text{ m}^3/\text{m}^3$
- Port 3: $0.012 \text{ m}^3/\text{m}^3$
- Port 4: $0.043 \text{ m}^3/\text{m}^3$

This data set is important to understand, because it showed how even at the lowest temperature in the cycle, there was still UVWC throughout the entire column in the case scenario with high water level.

5.1.4 UVWC Analysis:

As stated in section 4.1, one of the main objectives for the specific experiment was to figure out how the UVWC evolves in the saturated and unsaturated portions of the inert cover material under freezing soil conditions. The UVWC indicated the quantity of water that remained in its liquid state, and as stated under the comment section for each of the water levels, with the exception of port 4, at mid water level, the UVWC was not completely depleted at -8.0°C . The results of the experiment reinforce section 3.1, which described that water located within fine pores does not freeze, even below 0°C (Spaans & Baker, 1996).

Water level seemed to play a significant role in UVWC during freeze and thaw cycles. As observed in Figure 22, the initial and final UVWC measurements for most of the water levels seemed to start and end within the same range, with minor fluctuations in quantity for most ports, only really varying $0.01\text{m}^3/\text{m}^3$ to $0.05\text{m}^3/\text{m}^3$. An additional observation that may be made is that regardless of the initial height of the column, the quantity of UVWC decreased moving up the columns (from port 1 to port 4), in each of the 3 column scenarios. Meaning, port 1 seemed to always have a higher amount of UVWC in comparison to port 4. This may be due to the manner water behaved upon freezing in a stagnant location and the impact of porosity on the movement of UVWC. The UVWC at the freeze point of each of the ports in each water level also seemed to follow the same decline trend, decreasing in volume moving up the column.

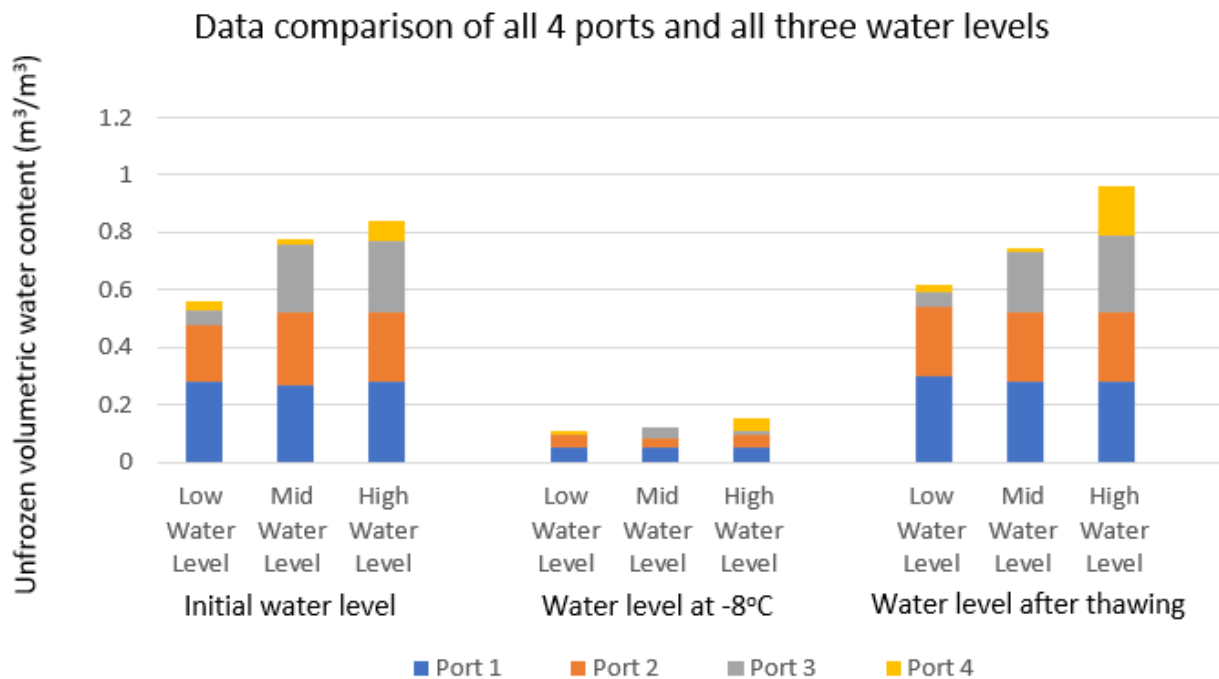


Figure 22: Data comparison of all 4 ports and all three water levels

Overall, it seemed as though the UVWC decreased moving up the column (from port 1 to port 4), the initial and final values for each of the ports in all 3 case scenarios were within the same range with very little variability, and at the coldest temperature in most of the cycles, there was still some amount of UVWC present. This may have been due to the granulometry of the sand and silica powder, a mesh sieve was initially used to determine particle-size distribution, but after altering water levels and running a few freeze and thaw cycles (swelling and un-swelling), it may have affected the granulometry within the column.

Data obtained from this analysis may be used to calculate D_e , using a method described in section 5.1, which may then be used to determine the O_2 flux. However, more freeze and thaw cycles need to be applied in order to see if no weathering of the material would occur. In the literature, it was identified that erosion of the cover material was linked with changes in soil properties such as the water retention curve, the apparition of preferential pathways following fluctuation of the solid material by ice, changes in granulometry and changes in the specific gravity of the particles. Overall, all those parameters are linked with the porosity and might affect the O_2 flux.

5.2 O_2 Concentration and Temperature

As stated in the materials and methods, 2 galvanic O_2 sensors (SO-110, Apogee Instrument Inc.) modified with diffusion heads were utilized to obtain the gaseous O_2 concentration in the partially saturated portion of the cover, for each of the two cycles. Figure 8 illustrates the way the O_2 sensors were positioned for their respective cycles. In the first cycle, the water level was closer to the bottom, one of the O_2 sensors was 2 cm below the surface of the cover material (near port 4), and the last sensor was placed 2 cm above the water interface (between port 1 and 2). In the second cycle, the water was closer to the middle, similar to the first cycle, one of the O_2 sensors was 2 cm below the surface of the cover material (near port 4), and the last sensor was placed 2 cm above the water interface (between port 2 and 3), see figure 1 in this text or section 4.2.2. By utilizing the data obtained from the three column experiments and the data from the O_2 sensors, the following observations were made about the O_2 migration within saturated covers. It should, however, be noted that there was a small quantity of data points to work with when it came to O_2 concentration data, so the trends should be considered estimates.

5.2.1 First Cycle: Low water level (Between port 1 and port 2)

From room temperature to the frozen point, the O_2 concentrations decreased for both the lower O_2 sensor and the upper O_2 sensor (Figure 23). Another characteristic both seemed to have in common is that nearing the end of the freeze, they both seem to have a jump in O_2 concentration. For the upper O_2 sensor, the O_2 concentration went from close to 16%, down to 14.5%, with the lowest O_2 concentration being 14.4% at -8.6°C , before jumping up to 14.5% at -8.7°C .

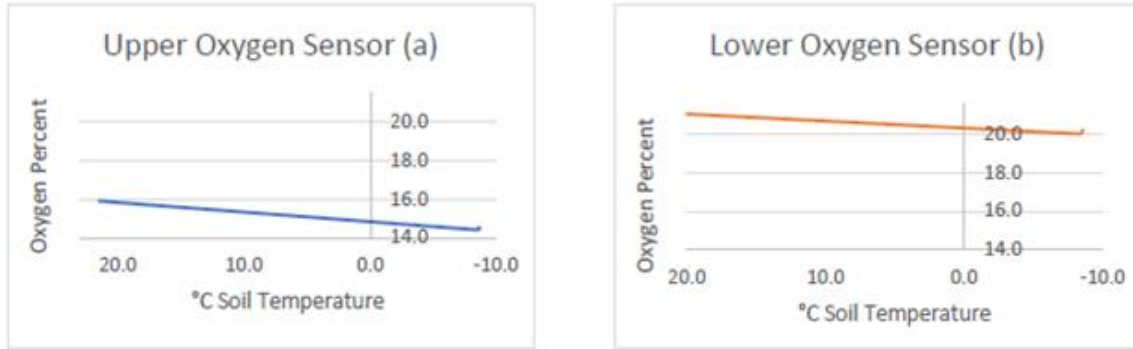


Figure 23: First cycle, low water level, Upper O₂ in freezing conditions: (a) Upper O₂ sensor, (b) Lower O₂ sensor

For the lower O₂ sensor, the O₂ concentration went from 21.2% down to 20.1%, with the lowest O₂ concentration being 20% at -8.4°C, before jumping up to 20.1% at -8.5°C.

Initial and final concentrations:

- Upper O₂ sensor: 16% (initial), 14.5% (final)
- Lower O₂ sensor: 21.2% (initial), 20.1% (final)

This indicated that while there is a decline in O₂ concentration as the temperature freezes, there is only a very slight decrease in the upper oxygen sensor for the column with a low water level.

5.2.2 Low water level: Unfrozen volumetric water content and O₂ concentration

The evolution of UVWC in port 1 (a) illustrated in Figure 22 during the freeze cycle (a) and the data obtained from the lower O₂ sensor, helped provide information regarding the effects of unfrozen water movement on O₂ concentration and therefore O₂ migration. Although UVWC and O₂ concentration did not have a parallel relationship, understanding the effects of temperature and volume of unfrozen volumetric water content in the ways they may impact the concentration of O₂ concentration is relevant in analyzing the O₂ flux.

5.2.3 Second Cycle: Mid water level (between port 2 and 3) Upper O₂ sensor

In the second cycle (Figure 24), the O₂ concentration for the upper O₂ sensor went from 20.8%, with a temperature of 20.5 °C, to 20.4% at -13.3°C, before going down to its lowest point at 20.1% at -8.6°C (Figure 24). From there the O₂ percent seemed to rise steadily as the temperature increased. It went from 20.1% to 20.4% in the span of around 13 degrees (-8°C to 21°C). The O₂ concentration then jumped dramatically up to 20.9% upon reaching room temperature.

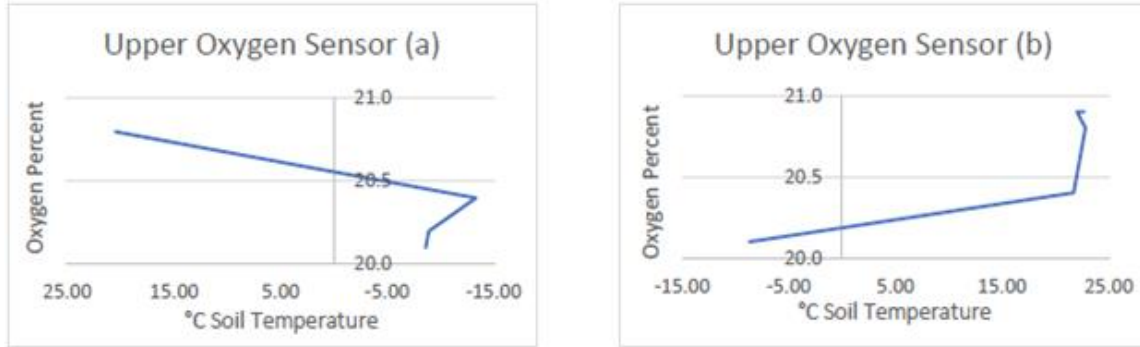


Figure 24: Second cycle, mid water level, Upper O₂: (a) freeze, (b) thaw

Initial and final concentrations:

- Upper O₂ sensor: 20.8% (initial), 20.9% (final), 20.1% (at the coldest point).

It appeared for the upper oxygen sensor with mid water level, the oxygen concentration only had mild fluctuations in temperature.

5.2.4 Second Cycle: Mid water level (between port 2 and 3) Lower O₂ sensor

From room temperature to -8.8°C (Figure 25), the O₂ concentration decreased fairly steadily, as it did for the upper O₂ sensor (Figure 25). The thaw for the lower sensor also seemed to be similar to the upper O₂ sensor: the O₂ concentration went from 16.6% at -8.7°C to 16.7, at 22.3°C before dramatically jumping up to 17.9% at 23°C.

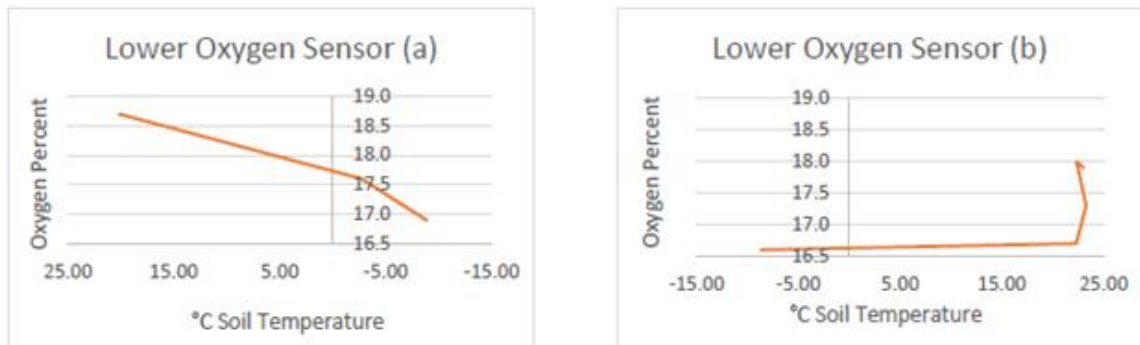


Figure 25: Second cycle, mid water level, Lower O₂: (a) freeze, (b) thaw

Initial and final concentrations:

- Lower O₂ sensor: 20% (initial), 17.9% (final), 16.6% (at the coldest point).

These values showed that in the second cycle, when the water was close to the middle, the O₂ concentration at the coldest point, as well as upon reaching room temperature after the coldest point seemed to be the lowest out of all of the other water levels and cycles.

5.3 O₂ Data Analysis

One of the objectives outlined in section 4.1 for the experiment was to predict the O₂ profiles in the low-level water column and the mid-level water column. By creating the above graphs, a few important conclusions may be made about the O₂ concentration, as temperature fluctuates.

Figure 22 illustrates how similar O₂ concentration fluctuations are for both the upper O₂ sensor and the lower O₂ sensor with low water level. They both had a consistent decline until reaching the coldest point. As for the second cycle, the upper and lower O₂ sensors seemed to be fairly similar in ways the O₂ fluctuated in both the freeze and thaw cycle. Going from room temperature to the freeze point, the O₂ for both declined steadily, until a specific point (around -13.3°C for the Upper O₂ sensor and -8.8°C for the lower sensor), where there was a steep decline in both temperature and O₂. The thaw cycle for the upper and lower O₂ sensor was also very similar, in the way the O₂ concentration increased moderately for the upper sensor, and very slightly for the lower sensor, until reaching a specific point (21.7°C for the upper O₂ sensor and 22.3°C for the lower O₂ sensor), where the O₂ concentration then spikes back up. The drastic fluctuations in O₂ concentration may be explained by the sensor's inability to measure the O₂ concentration on frozen material, and be based on the quantity of UVWC. This was seen by the small quantity of O₂ points that were measured during the experiment. It is also important to understand that the galvanic cell sensors consumed 2.2 μmol O₂/day. While the experiments were completed as fast as possible, this may have caused some fluctuations in the results.

6 Conclusions

6.1 Limitations

Considering the approach chosen to investigate the migration of oxygen in the saturated cover, some limitations were likely inherent to the study. D_e was supposed to be estimated from Aachib et al.'s (2004) equation adapted for temperature (Equation 11) as described in the experimental protocol, however due to the complexity of the equations involved and calculation variables that were not accounted for during the experimental stage, data results were directly analysed with the utilization of multiple unfrozen volumetric water content and oxygen graphs. Also, it was not possible to make use of the normal functionality of Vadose/W because the software did not allow analysis for temperatures under 0°C, as indicated by the user guide. Values would need to be implied from theoretical models and manually forced to represent the actual freezing conditions, which could result in some uncertainties in the calculated flux. However, since the oxygen gradient was supposed to be measured in the unfrozen portion for calibration purposes, the uncertainties mainly concerned the fully saturated portion of the cover (below the water table level). Finally, it should be noted that the fully submerged portion likely underwent some swelling since the initial degree of saturation was more than 91.7% (a threshold described in Nyamego, 2017). Swelling also affected the measurement of volumetric water content though changes in the porosity of the frozen solid sample, volumetric air content and other parameters of interest of the samples. Thus, only an approximation of the flux reaching the tailings could be provided by this study.

6.2 Summary of Results

It appears as though both the O₂ concentration and UVWC seem to follow similar trends. The UVWC decreases moving up the column (from port 1 to port 4), the initial and final values for each of the ports in

all 3 case scenarios are within the same range with very little variability, and at the coldest temperature in most of the cycles, there is still some amount of UVWC present. The UVWC graphs also seem to present regions of UVWC stability, until reaching a specific value, where the UVWC seems to drop (in the freeze cycle) or rise (in the thaw cycle) suddenly, before leveling out again. This is expected, as the drop and rise in UVWC seem to be near the freezing point of water and the melting point of ice.

For the O₂ concentration, we again see similar regions presented throughout most of the O₂ cycles. In this case, there seems to be an overall gradual decline in O₂ concentration, and a slight jump of O₂ concentration nearing the end of the cycle. It should, however, be noted that there was a rather small quantity of data points to work with when it came to O₂ concentration data, so the trends should be considered estimates.

Similarly, for both the UVWC and the O₂ concentration more freeze and thaw cycles need to be applied in order to see if no weathering of the material would occur. In this case the experiment was only performed once due to the limitations of the equipment used, but perhaps a future experiment with more cycles may allow for a better understanding of the effects of multiple freeze and thaw cycles on the UVWC and the O₂ concentrations.

6.3 Conclusions

The objectives of this study were to evaluate the impact of freeze-thaw cycles on oxygen migration within saturated covers over tailings, by simulating a tailing cover system in the laboratory through column experiments. UVWC and O₂ concentration were monitored in different scenarios where water level varied and through freeze and thaw cycles.

From the results presented above, it appears that **water level seems to play a significant role in UVWC during freeze and thaw cycles.**

UVWC and O₂ concentration do not have a linear relationship, they appear to follow similar trends.

A steady decline of UVWC content within each of the three column scenarios was observed; regardless of the height of the water the UVWC decreases moving up the column.

Port 1 seems to always have a higher volume of UVWC in comparison to port 4. This may be due to the manner water behaves upon freezing in a stagnant location and the impact of **porosity** on the movement of UVWC.

At the coldest temperature in most of the cycles (around -8°C), there is still some amount of UVWC present, which means that **oxygen diffusion may be still possible even at cold temperature** in these unfrozen parts of the saturated cover.

6.4 Subsequent Experiment

Due to the unforeseen limitations to this experiment, a future in-depth lab-scale study inspired by the double chamber cell test is also planned to help provide a more realistic analysis of the effects of water level, and freeze-thaw phenomenon on oxygen migration in saturated covers. The subsequent study will focus on the utilization of techniques that may allow the direct measurement of oxygen diffusion through inert materials without needing variables to assume the quantity of oxygen. This will allow a more accurate estimation of oxygen diffusion in actual saturated covers.

7 References

- Aachib, M., Mbonimpa, M., Aubertin, M. (2004). Measurement and prediction of the oxygen diffusion coefficient in unsaturated media, with applications to soil covers. *Water, Air, and Soil Pollution*, 156: 163-193.
- Aubertin, M., Cifuentes, E., Apithy, S. A., Bussière, B., Molson, J., & Chapuis, R. P. (2009). Analyses of water diversion along inclined covers with capillary barrier effects. *Canadian Geotechnical Journal*, 46(10), 1146-1164. doi:10.1139/t09-050
- Aubertin, M., Bussière, B., Monzon, M., Joanes, A.-M., Gagnon, D., Barbera, J.-M., Aachib, M., Bedard, C., Chapuis, R.P., Bernier, L. (1999). Étude sur les barrières sèches construites à partir des résidus miniers. – Phase II : Essais en place. Projet CDT P1899, MEND 2.22.2c, 331 pages.
- Barbour, S. L., Lim, P. C., et Fredlund, D. G. (1996). A new technique for diffusion testing of unsaturated soil. *Geotechnical Testing Journal*, 19(3), 247-258.
- Bussière, B., Benzaazoua, M., Lelièvre, J., Bois, D., et Servant, S. (1998). Valorisation des résidus miniers: une approche intégrée - Phase II. Rapport final soumis au Ministère des Ressources Naturelles du Québec. MEND Program, Rouyn-Noranda, Québec.
- Bussière, B., Benzaazoua, M., Aubertin, M., et Mbonimpa, M. (2004). A laboratory study of covers made of low sulphide tailings to prevent acid mine drainage. *Environmental Geology*, 45, 609-622.
- Binning, P.J., Postma, D., Russell, T.F., Wesselingh, J.A., Boulin, P.F. (2007). Advective and diffusive contribution to reactive gas transport during pyrite oxidation in the unsaturated zone. *Water Resources Research*, 43, WO2414.
- Collin, M. (1987). Mathematical modeling of water and oxygen transport in layered soil covers for deposits of pyritic mine tailings. *Licenciate Treatise*. Department of Chemical Engineering, Royal Institute of Technology, Stockholm, Sweden.
- Collin, M. and Rasmuson, A. 1988. Gas diffusivity models for unsaturated porous media. *Soil Science America Journal*, 52: 1559-1565.
- Cosset, G. (2009). Comportement hydrogéologique d'une couverture monocouche sur des résidus miniers sulfureux : essais en colonne et simulations numériques. Master thesis, Mineral Engineering, École Polytechnique Montréal offered in extension at UQAT (Université du Québec en Abitibi-Témiscamingue)
- Coulombe, V. (2012). Performance de recouvrements isolants partiels pour contrôler l'oxydation de résidus miniers sulfureux. Master thesis, Mineral Engineering, École Polytechnique Montréal offered in extension at UQAT (Université du Québec en Abitibi-Témiscamingue).
- Dagesse, D.F. (2010). Freezing-induced bulk soil volume changes. *Canadian journal of soil science*, 90(3)m 389-401.
- Davé, N., Blanchette, M., & Giziewicz, E. (1996). Review and assessment of the roles of ice, in the water cover option, and permafrost in controlling acid generation from sulphide tailings. MEND Program. Previsions report, 1(1). 96 pages

- Davé, N.K. (2017). Knowledge Gaps in Water Cover and Saturated Cover Mine Waste Management Technologies. CanmetMining Report. CMIN 2016-xxxx-RP, September 2016, National Resources Canada, December 2000.
- David, D. J., et Nicholson, R. V. (1995). Field measurements for determining rates of sulphide oxidation. Sudbury '95, Conference on Mining and the Environment, Sudbury, Ontario, 201-210.
- Demers, I. (2008), Performance d'une barrière à l'oxygène constituée de résidus miniers faiblement sulfurés pour contrôler la production de drainage minier acide. Ph.D thesis, Université du Québec en Abitibi Témiscamingue, Abitibi Témiscamingue, Canada.
- Demers, I., Bussière, B., Benzaazoua, M., Mbonimpa, M., & Blier, A. (2010). Preliminary optimization of a single-layer cover made of desulphurized tailings: application to the Do yon Mine tailings impoundment. Society for Mining, Metallurgy, and Exploration Annual Transactions, 326, 21-33.
- Denny, M. W. (1993). Air and water: the biology and physics of life's media: Princeton University Press.
- Elberling, B., Nicholson, R. V., et Scharer, J. M. (1994). A combined kinetic and diffusion model for pyrite oxidation in tailings: a change in controls with time. *Journal of Hydrology* (157), 47-60.
- Elberling, B. (2005). Temperature and oxygen control on pyrite oxidation in frozen mine tailings. *Cold Regions Science and Technology*, 41(2), 121-133.
- El-Farhan, Y. H., Petersen, L. W., Rolston, D. E., et Glauz, R. D. (1996). Analytical solution for two-region diffusion with two well-mixed end chambers. *Soil Science Society of America Journal*, 60, 1697-1704.
- Fredlund, D.G., Xing, A., (1994). Equations for the soil-water characteristic curve. *Canadian Geotechnical Journal*, 31, 521-532.
- Glauz, R. D., et Rolston, D. E. (1989). Optimal design of two-chamber, gas diffusion cells. *Soil Science Society of America Journal*, 53(6), 1619-1624.
- Gosselin, M. (2007). Étude de l'influence des caractéristiques hydrogéochimiques des résidus miniers réactifs sur la diffusion et la consommation de l'oxygène. Master's thesis, département des génies civil, géologique et des mines, Polytechnique de Montréal, Québec, Canada.
- Hamdi, J. (2011). Mesures expérimentales des concentrations en oxygène sur le terrain et modélisation numérique pour évaluer le flux de diffusion dans la couverture du site minier LTA. Master thesis, Mineral Engineering, École Polytechnique Montréal offered in extension at UQAT (Université du Québec en Abitibi-Témiscamingue).
- Hillel, D. (1998). Environmental soils physics. Academic press Inc, New York.
- Li, M., Catalan, L. (1997). Desulphurization of Golden Giant CIP tailings - Progress report no.5: Assessment of acid generation potential and cover effectiveness of depyritized tailings. Noranda Technology Centre, Pointe-Claire.
- MacKay, P.L., Yanful, E.K., Rowe, R.K., Badv, K. 1998. A new apparatus for measuring oxygen diffusion and water retention in soils. *Geotechnical Testing Journal*, 21 (4): 289-296
- Marshall, T.J. (1959). The diffusion of gas in porous media. *Journal of Soil Science*, 10: 79-82.

- Mbonimpa, M., Aubertin, M., Aachib, M., Bussière, B. (2002). Oxygen diffusion and consumption in unsaturated cover materials. Report EPM-RT-2002-04, École polytechnique de Montréal, 55 pages.
- Mbonimpa, M., Aubertin, M., Aachib, M., Bussière, B. (2003). Oxygen diffusion and consumption in unsaturated cover materials. *Canadian Geotechnical Journal*, 40: 916-932.
- Mbonimpa, M., Aubertin, M., & Bussière, B. (2011). Oxygen consumption test to evaluate the diffusive flux into reactive tailings: interpretation and numerical assessment. *Canadian Geotechnical Journal*, 48(6), 878-890. doi: 10.1139/t11-015.
- MEND. (2001). Evaluation of man-made subaqueous disposal option as a method of controlling oxidation of sulphide minerals: Column studies. MEND program. Report 2.12.1e
- MEND. (2006). Update on Cold Temperature Effects on Geochemical Weathering. MEND program. Rapports 1.61.6.
- Millington, R.J., Quirk, J.P. (1961). Permeability of porous solids. *Faraday Society Transport*, 57: 1200-1206.
- Millington, R.J., Shearer, R.C. (1971). Diffusion in aggregated porous media, *Soil Science*, 111: 372-378.
- Nicholson, R.V., Gillham, R.W., Cherry, J.A., Reardon, E.J. (1988). Pyrite oxidation in carbonate-buffered solution, 1, experimental kinetics. *Geochimica et Cosmochimica Acta*, 50: 1509-1520
- Nicholson, R.V., Gillham, R.W., Cherry, J.A., Reardon, E.J. (1989). Reduction of acid generation in mine tailings through the use of moisture-retaining layers as oxygen barriers. *Canadian Geotechnical Journal*, 26: 1-8.
- Nyameogo, G. (2017). Développement d'un système de mesure et d'un modèle théorique préliminaire d'estimation du coefficient de diffusion de l'oxygène dans les matériaux poreux inertes gelés. Master's thesis, département des génies civil, géologique et des mines, Polytechnique de Montréal, Québec, Canada.
- Ouangrawa, M. (2007). Étude expérimentale et analyse numérique des facteurs qui influencent le comportement hydro-géochimique de résidus miniers sulphureux partiellement submergés. Ph.D thesis, École Polytechnique de Montréal, Montréal, Canada
- Pétel, K. (2017). Évaluation en laboratoire de recouvrements spécifiquement adaptés au contrôle du drainage neutre contaminé. Ph.D thesis, École Polytechnique de Montréal, Montréal, Canada.
- Reid, R., Prausnitz, J., & Sherwood, T. (1977). *The Properties of Glass and Liquids* Third, Edition: McGraw-Hill Book Company, New York, NY.
- Richards, L.A. (1931). Capillary conduction of liquids through porous medium. *Journal Physics*. 1, 318-333.
- Richards, T. (1969). Calculating the oxygen diffusion coefficient in water
- Sallam, A., Jury, W. A., et Letey, J. (1984). Measurement of gas diffusion coefficient under relatively low air-filled porosity. *Soil Science Society of America Journal*, 48, 3-6.
- Sander, S. P., Burkholder, J. B., Abbatt, J. P. D., Barker, J. R., Huie, R. E., Kolb, C. E., Kurylo, M. J., Orkin, V. L., Wilmouth, D. M., Wine, P. H. (2006). Chemical kinetics and photochemical data for use in atmospheric studies evaluation number 15.

- Sander, R. (2015). Compilation of Henry's law constants (version 4.0) for water as solvent. *Atmospheric Chemistry & Physics*, 15(8).
- Shelp, M. L., et Yanful, E. K. (2000). Oxygen diffusion coefficient of soils at high degrees of saturation. *Geotechnical Testing Journal*, 23(1), 36-44.
- Spaans, E. J., & Baker, J. M. (1996). The soil freezing characteristic: Its measurement and similarity to the soil moisture characteristic. *Soil Science Society of America Journal*, 60, 13- 19.
- Yanful, E.K. (1993). Oxygen diffusion through soil covers on sulphidic mine tailings. *Journal of Geotechnical Engineering, ASCE*, 119(8): 1207–1228.

Appendix A: Unfrozen Saturated Media Equations

Flow of water in saturated and unfrozen porous media

In a saturated porous medium, only two phases are present, namely the liquid phase and the solid phase. The determination of the flow velocity of the fluid between two points can be made from Darcy's law, such as:

$$q = -k * i \quad (\text{eq.13})$$

Where q is the specific flow [LT^{-1}], k is the hydraulic conductivity [LT^{-1}] and i is the hydraulic gradient [LL^{-1}]. The hydraulic gradient i also reflects the variation of the hydraulic load as a function of the distance which, in the one-dimensional case, is recorded as

$$i = \frac{\partial h}{\partial z} = \frac{h_a - h_b}{L} \quad (\text{eq.14})$$

The hydraulic load h [L] can also be determined using the Bernoulli water potential equation, neglecting the velocity term (considered to be very low). The determination of the saturated hydraulic conductivity can also be done experimentally from a flexible or rigid-walled permeameter or from a predictive model such as that of Kozeny-Carman or modified Kozeny-Carman.

The law of conservation of the mass must also be used in order to define the movement of water in a solid matrix. This law stipulates that for a rigid material, the specific flow q that leaves a volume of soil must be equal to that entering:

$$\text{div } \vec{q} = 0 \quad (\text{eq.14})$$

In the case of an anisotropic soil, the generalization of 3-dimensional equations through a matrix system becomes essential to define the hydraulic conductivity of the soil in all directions.

Appendix B: Unfrozen Unsaturated Media Equations

Flow of water in partially saturated and unfrozen porous media

Based on the equations describing flows in a saturated medium, Richards (1931) developed an equation that solves the problems of water flow in an unsaturated medium, such as:

$$\frac{\partial \theta}{\partial t} = -\frac{\partial}{\partial x} \left[k_x(\psi) \frac{\partial \psi}{\partial x} \right] - \frac{\partial}{\partial y} \left[k_y(\psi) \frac{\partial \psi}{\partial y} \right] - \frac{\partial}{\partial z} \left[k_z(\psi) \frac{\partial \psi}{\partial z} \right] + \frac{\partial}{\partial z} k_z(\psi) \quad \text{eq.15}$$

Where θ corresponds to the volumetric water content, k_i is the hydraulic conductivity along the 3 reference axes and ψ is the suction resulting from the fact that above the water table level, the interstitial water pressure is lower than the atmospheric pressure. Thus, unlike the saturated case, there is a variation in the water content as a function of the suction (or water retention curve) and a variation of the hydraulic conductivity as a function of the suction (or function of permeability).

Water retention curve

The volumetric water content (θ_w) and the air volume content (θ_a) make it possible to quantify the proportions of water and air present in the pores of an unsaturated and unfrozen soil (reactive tailings or cover). These parameters are presented in the following equations 16 and 17.

$$\theta_w = \frac{V_w}{V_t} = n S_r = w(1 - n) \frac{\gamma_s}{\gamma_w} \quad (\text{eq.16})$$

$$\theta_a = \frac{V_a}{V_t} = n - \theta_w = (1 - S_r)n \quad (\text{eq.17})$$

Where n represents the porosity of the soil, S_r is the degree of saturation, V_i is the volume of air or water or total, γ_i is the density of the soil/water. It is the phenomenon of water retention by capillarity (in the pores of a soil) which is at the origin of the water contents which will be observed in an unsaturated medium. In order to be able to experimentally link the amount of water that a soil can retain within its pores (degree of saturation) depending on the height of the water table (suction), the use of a Tempe cell is often preferred. This experimental method consists of making point measurements of the suction necessary for the desaturation of the soil for various degrees of saturation. In addition to this method, predictive models based on soil geotechnical properties (void index, grain size, etc.) can be used to construct the water retention curve. Figure B1 shows an example of a water retention curve for a fictive material.

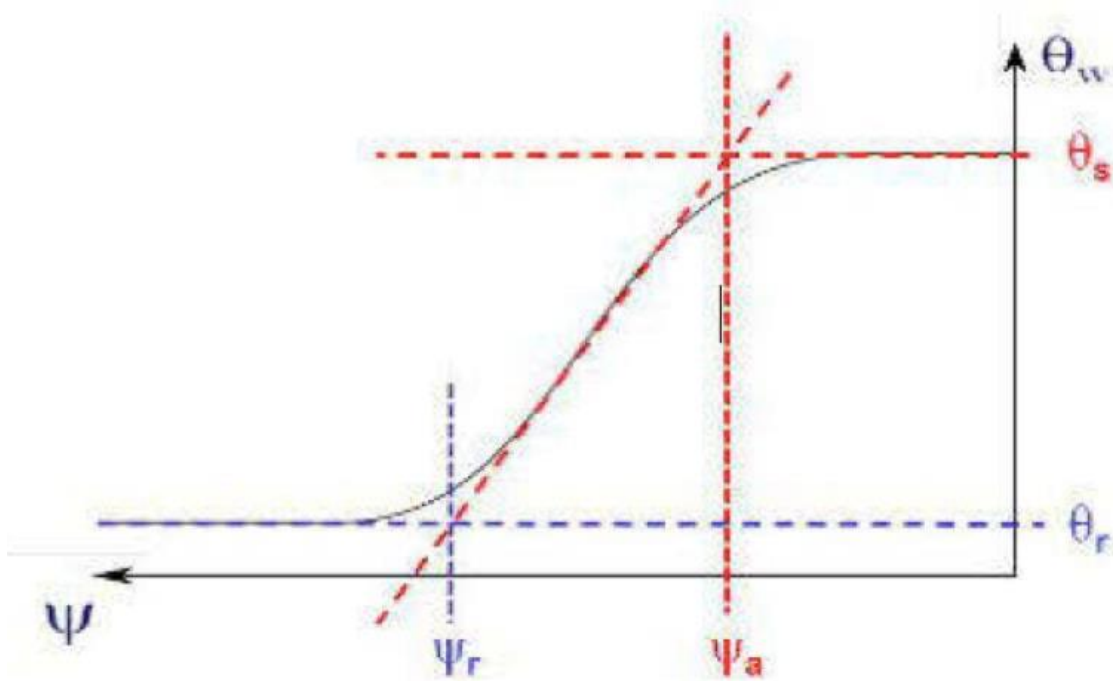


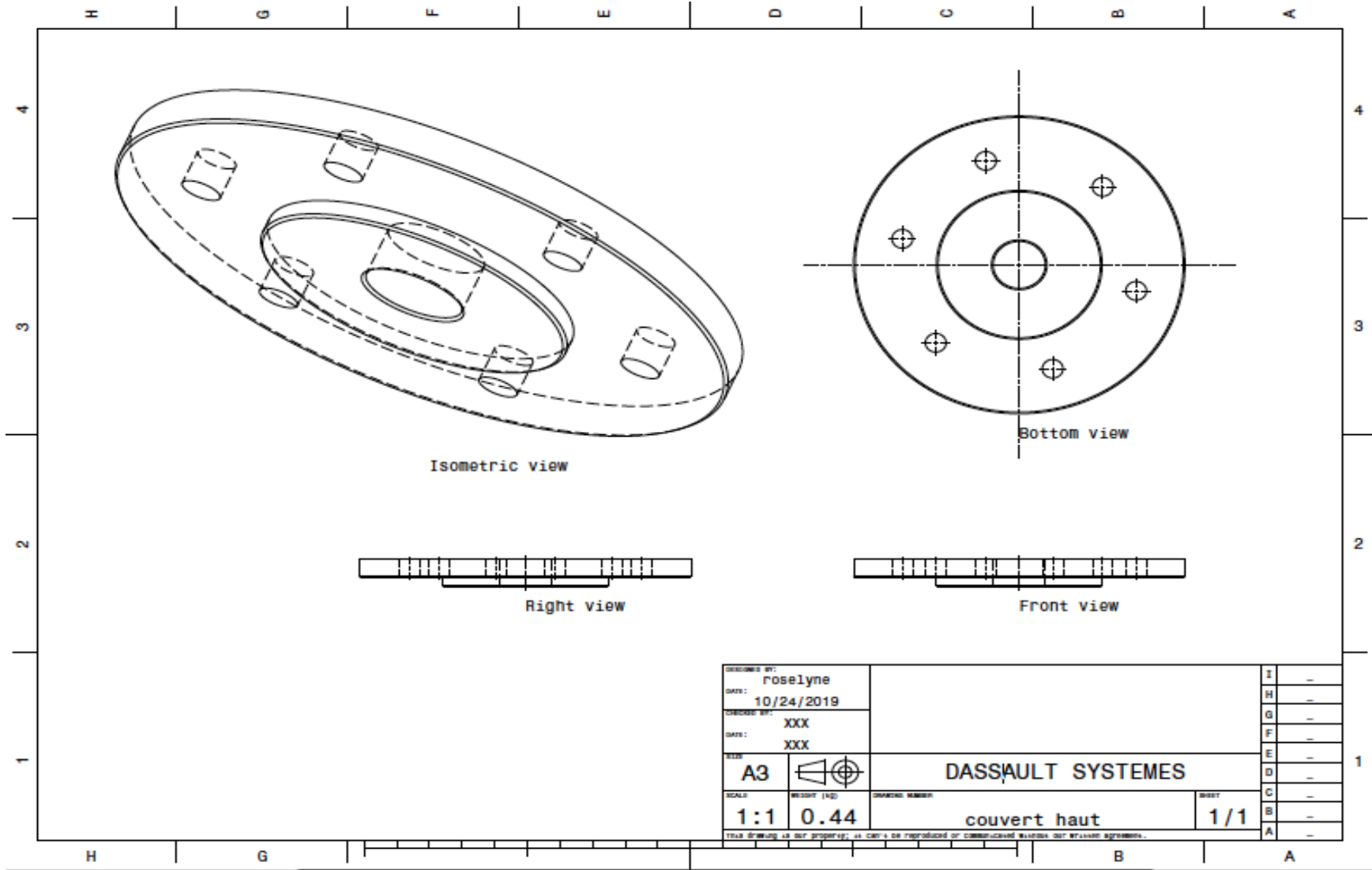
Figure B1 Water retention curve (Cossett, 2009)

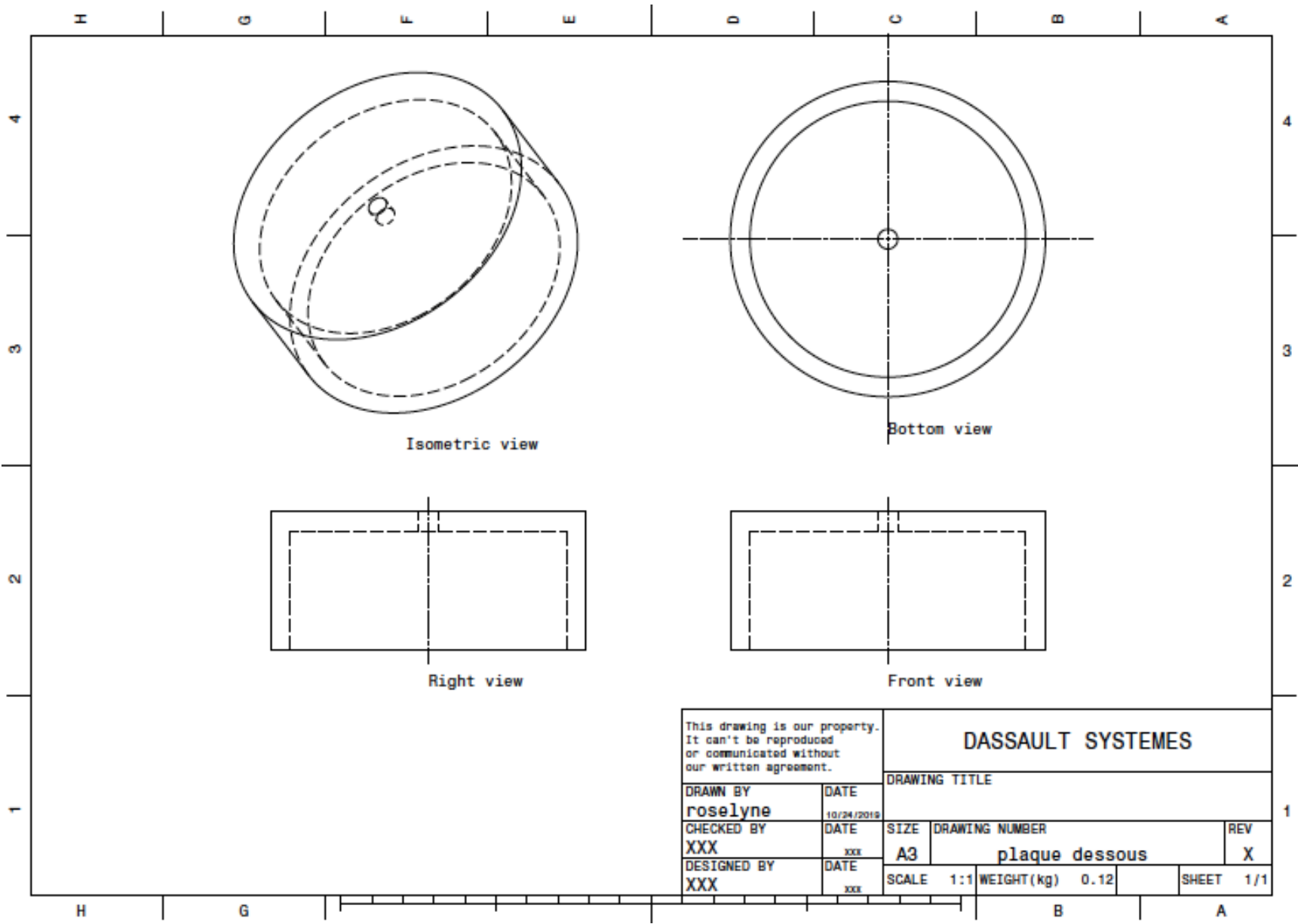
Finally, two important characteristics of the material can be deduced from the graph, namely the air entry value (AEV, ψ_a) and the water entry value (WEV, ψ_r). ψ_a corresponds to the suction which is greater than the capillary tension of the pores, from which we can see the beginning of the desaturation of the studied material. ψ_r corresponds to the suction that is observed when the volume content of the material is equal to the water content of the soil.

Permeability function

This relation expresses the variation of the hydraulic conductivity k as a function of the suction experienced by the medium ψ . This suction also reflects the degree of saturation of the corresponding soil. Thus, when the soil has a high water content, its pores will be filled with water and water can flow easily through it: a high hydraulic conductivity will be observed. Otherwise, for a low degree of saturation, the pores will be filled with air, which will reduce the hydraulic conductivity. In short, the air acts as a brake on the flow. Note that the permeability function can be determined experimentally from cell permeability tests or estimated from the water retention curve and the saturated hydraulic conductivity.

Appendix C: Double-Chamber Cell Design

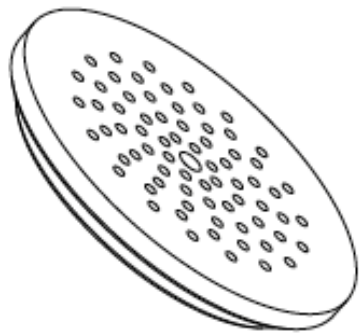




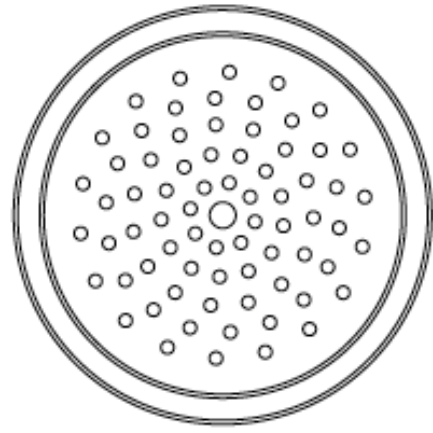
This drawing is our property. It can't be reproduced or communicated without our written agreement.		DASSAULT SYSTEMES		
DRAWN BY roselyne		DRAWING TITLE		
DATE 10/24/2019	CHECKED BY XXX	DATE xxx	SIZE A3	DRAWING NUMBER plaque dessous
DESIGNED BY XXX	DATE xxx	SCALE 1:1	WEIGHT (kg) 0.12	REV X
			SHEET 1/1	

H G F E D C B A

4



Isometric view



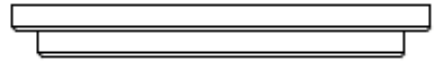
Bottom view

3

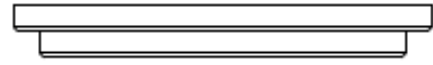
3

2

2



Right view



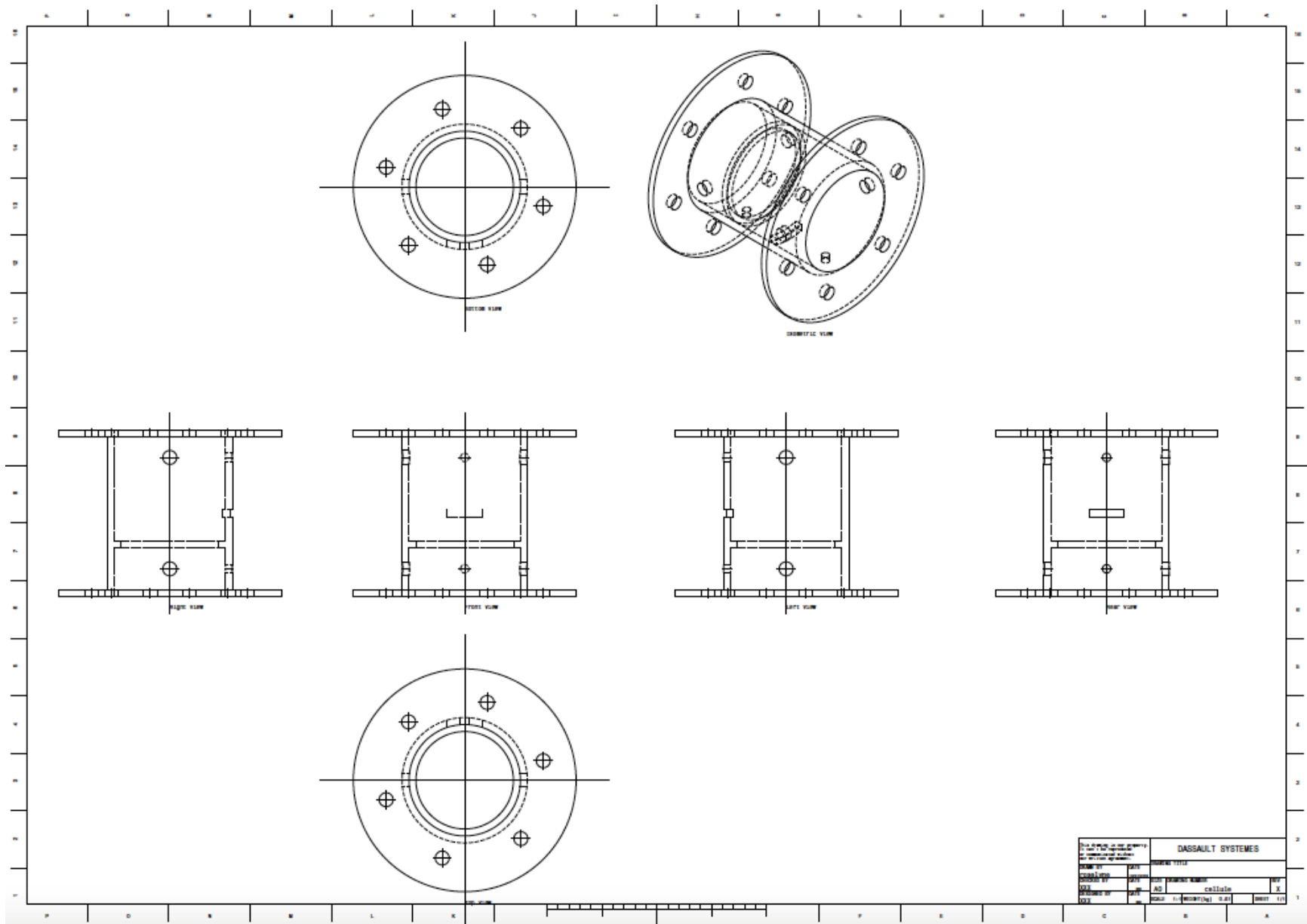
Front view

1

1

This drawing is our property. It can't be reproduced or communicated without our written agreement.		DASSAULT SYSTEMES			
DRAWN BY roselyne		DRAWING TITLE			
DATE 10/24/2019	SIZE A3			DRAWING NUMBER plaque perforée	REV X
CHECKED BY XXX	DATE xxx	SCALE 1:1	WEIGHT(kg) 0.08	SHEET 1/1	
DESIGNED BY XXX	DATE xxx				

H G B A



DASSAULT SYSTEMES <small>15, rue de l'Éclairage 92265 La Garenne-Maisons Cedex 13 - France</small>		DASSAULT SYSTEMES ORGANISATION	
DRAWN BY CDD/ADP CHECKED BY CDD/ADP	DATE 01/01/01	PROJ. NUMBER AD	PART NUMBER calliste
DRAWN BY CDD	DATE 01/01/01	PROJ. NUMBER AD	PART NUMBER calliste